HHS Public Access

Author manuscript

Chem Soc Rev. Author manuscript; available in PMC 2019 April 03.

Published in final edited form as:

Chem Soc Rev. 2018 April 03; 47(7): 2280–2297. doi:10.1039/c7cs00522a.

Organic molecule-based photothermal agents: An expanding photothermal therapy universe

Hyo Sung Jung[a,b,‡], **Peter Verwilst**[a,‡], **Amit Sharma**[a], **Jinwoo Shin**[a], **Jonathan L. Sessler**[b,c], and **Jong Seung Kim**[a]

[a]Department of Chemistry, Korea University, Seoul 02841, Korea

[b]Department of Chemistry, The University of Texas at Austin, Austin, Texas 78712-1224, USA

[c]Center for Supramolecular Chemistry and Catalysis, Shanghai University, Shanghai 200444, China

Abstract

Over the last decade, organic photothermal therapy (PTT) agents have attracted increasing attention as a potential complement for, or alternative to, classical drugs and sensitizers involving inorganic nanomaterials. In this tutorial review, we provide a structured description of the main classes of organic photothermal agents and their characteristics. Representative agents that have been studied in the context of photothermal therapy since 2000 are summarized and recent advances in using PTT agents to address various cancers indications are highlighted.

Graphical Abstract

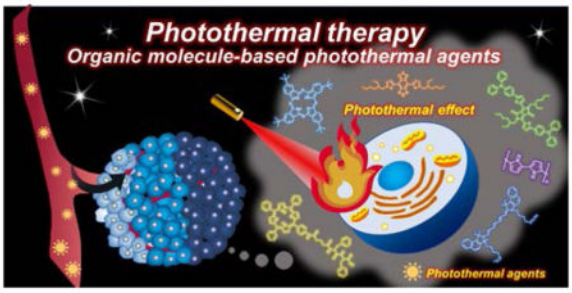

1. Introduction

Photothermal therapy (PTT), as its name implies, is a treatment that involves the artificial elevation of the tissue temperature. It takes advantage of the susceptibility of cells towards heat to induce apoptosis or increase sensibility to radio-or chemotherapy.[1] PTT has shown particular promise in the area of cancer therapy. Compared with conventional cancer treatment modalities, such as surgery, radiotherapy and chemotherapy, PTT is attractive because of its potential for high inherent specificity and a lower invasive burden. In

Correspondence to: Jonathan L. Sessler; Jong Seung Kim.

‡These authors contributed equally to this work.

principle, PTT can also provide a cancer treatment that does relatively little damage to surrounding healthy tissues. This is because the thermal effect is produced only when near-infrared (NIR) light is applied and only in the presence of a PTT agent.[2] Through appropriate design, PTT agents can be specifically targeted to the cancer site, further enhancing the selectivity.

Given the fact that molecular design plays such a critical role in the success of PTT, it is not surprising that considerable effort has been devoted to the development of ever-better sensitizing agents. To date, most of this effort has focused on NIR light-triggered inorganic materials, including transition metal nanoparticles, sulfide nanoparticles, gold nanoparticles, and platinum nanoparticles.[2] While these systems as a general rule show favorable absorbance features, excellent photothermal conversion efficiencies, and good photo-stabilities, their lack of biodegradability and potential for long-term toxicity have provided barriers to effective clinical translationefforts.[3]

In recent years, small organic molecules have received increasing attention as potential alternatives to nanomaterials in the area of PTT. These molecular sensitizers typically function by absorbing photons produced by NIR irradiation. They then generate heat through non-radiative relaxation pathways.[4] A potential advantage of organic PTT sensitizers lies in the fact that, unlike inorganic materials, organic-based materials can be designed with considerations of safety and formulation in mind. Their features can be further fine-tuned through dedicated synthesis. For instance, organic agents can be modified so as to function as theranostics, a descriptor that encompasses constructs that allow for simultaneous imaging (by, e.g., fluorescent or photoacoustic means)and photothermal -basedtherapy.[4]

A further particularly attractive aspect of organic-based PTT agents is that they may permit cancer targeting.[4,5,6] Strategies in common use in this context include passive targeting,[8,10–12,19–21,24–27,32,33,35–47,49] active targeting,[9,13,48] stimuli-controlled strategies,[15] subcellular targeting,[14,23] and combinational strategies.[11,27,40,44] Collectively, these approaches have been exploited in PTT agents that rely on cyanines,[8–23] diketopyrrolopyrroles,[24–27] croconaines,[28–31] porphyrins,[32–35] polymers,[37–46] and several other agents[47–50] as the photothermal payload (Fig. S1, ESI†). Considerable progress has been made using molecules of these various classes. Nevertheless, improvements in the photothermal conversion efficiency and bio -and photo -stability are likely to be needed before a clinically viable set of candidates emerges. In light of this, substantial efforts have been devoted to the development of advanced organic photothermal agents, capable of delivering heat to an affected target site. This review is designed to summarize these recent efforts. Key features of the PTT agents discussed in this review are summarized in Table 1. A visual overview of key agents is provided in Fig. S1 in the Supporting Information.

2. Design and working principle of organic PTT agents

Following photoexcitation, most organic species undergo rapid internal conversion to the lowest excited singlet state (S_1). This latter state can decay back to the ground state by emitting a photon (fluorescence) or through nonradiative relaxation pathways. Intersystem

crossing to a triplet state, typically T_1, is also possible. Photothermal effects (i.e., heat generation) generally arise as the result of nonradiative relaxation processes (Scheme 1). These may be unimolecular or induced by collisions between the excited singlet species and its surroundings.

Ideally, organic photothermal agents should be able to fulfill four critical requirements: i) absorb strongly in the NIR region (to promote effective light absorption in a physiologically more transparent spectral region) while displaying low fluorescence quantum yield (FL-QY) and singlet oxygen generation yields (SO-QY) so as to maximize the conversion of absorbed photons to heat, ii) be nontoxicin the absence of photoirradiation yet kill cancer cells selectively under conditions of NIR illumination, iii) degrade quickly after use (so to improve safety), and iv) be easy to prepare and modify. To date, a number of organic dyes, including cyanines[8–23] and diketopyrrolopyrroles,[24–27] as well as some polymers,[37–46] have been found to satisfy many of these requirements and have been studied as potential PTT agents.

3. Cyanine-based agents

3.1. Indocyanine green-based agents

Indocyanine green (ICG) (Fig. 1A) is the quintessential NIR-absorbing PTT agent. It is endowed with excellent light-to-heat conversion efficiency. ICG is also an effective photodynamic therapy (PDT) sensitizer that produces reactive oxygen species (ROS) upon photoirradiation and shows a strong ultrasound response when used in the context of sonodynamic therapy. ICG has been approved by US Food and Drug Administration (FDA) as an optical imaging agent.[7] Since ICG exhibits NIR fluorescence, it is attractive as a so-called theranostic wherein diagnosis (fluorescence) is combined with therapy (PTT). However, therapeutic applications of ICG have been limited due to its poor bio-environmental stability, propensity to aggregate in aqueous media, lack of target specificity, and rapid clearance from the body.[7] However, improved efficacies have been obtained *via* encapsulation of ICG as described below.

Yoon *et al.* investigated liposomal formulations of ICG and optimized their PTT efficacy as a function of lipid composition and degree of ICG loading (Fig. 1B).[8] An optimized formulation (lipid/ICG composition, DMPC:PEG-PE:ICG = 950:50:4), shown as **1** in Fig. 1, produced an efficient PTT effect (an increase of 15 °C from an initial temperature of 25 °C within 1 min of irradiation using a 808 nm laser at 1.1 W/cm^2) with relatively low ROS production. The PTT conversion efficiency of the formulation was found to be ~8.99%; that is almost twice the level seen for free ICG (3.37%). Intratumoral injection of **1** in 4T1-tumor bearing mice (25 μg/mL, 50μL), followed by irradiation (15 min, 808 nm laser, 0.6 W/cm^2), resulted in a dramatic temperature increase (i.e., >50 °C). Using formulation **1** in conjunction with irradiation led to a reduction in the tumor burden in 4T1 tumor bearing mice relative to what was seen for free ICG or other ICG formulations. Owing to the residual ICG fluorescence, **1** also allowed for optical imaging (in addition to good therapeutic efficiency)in a mouse model of lymph node metastasis.

Zheng *et al.* used ICG in conjunction with nanoparticles endowed with cancer targeting moieties (Fig. 1C).[9] Here the ICG-bearing PL-PEG aggregates **2** were decorated with either folic acid **3** or a mAb directed at the $\alpha_v\beta_3$ receptor **4**. Upon irradiation (2 min, 808 nm laser, 1.25 W/cm^2) of a 0.05 mg/mL suspension of the nanoparticles in water, a temperature enhancement (ΔT = 22 °C) was observed. This formulation was also found to increase the stability of ICG in various biomimetic environments. The active targeting of **3** and **4** to their respective targets followed by PTT treatment (5 min, 808 nm laser, 2.75 W/cm^2) resulted in dramatic cytotoxicity in FR(+) EMT6 (~75%) and U87-MG(~90%) cells, respectively.

By coating ICG loaded PLGA (poly(lactic-co-glycolic acid)) nanoparticles with a homologous cancer cell membrane, Chen *et al.* constructed the biocompatible PTT agent **5** (Fig. 1D).[10] Useful features, such as long-term blood circulation times and evasion of an immune response due to the presence of self-antigens, were seen. Using these constructs, real-time dual fluorescent or photoacoustic imaging and efficient PTT cancer growth suppression could be achieved. In PBS solution under photoirradiation (8 min, 808 nm laser, 1 W/cm^2), a temperature increase by ~49 °C from an initial 25 °C value was observed.

Zheng *et al.* demonstrated the feasibility of using a dual PTT and chemotherapeutic approach to overcome resistance to doxorubicin (DOX) in cancer models (Fig. 1E).[11] In this study, lipid-polymer nanomaterials containing ICG and DOX (**6**) were used a PTT agent. A temperature increase to ~53 °C was seen upon irradiation (5 min, 808 nm laser, 1 W/cm^2). Significant cytotoxicity in both DOX-sensitive (MCF-7) and DOX-resistant (MCF-7/ADR) cell lines was seen, while attenuated tumor growth was achieved in the corresponding mouse xenograft tumor models. These findings were ascribed to synergistic combination of chemotherapy and PTT.

3.2. Heptamethine cyanine-based agents

Heptamethine dyes (Fig. 2A) are structurally related to ICG and have been tested extensively in PTT applications. Relative to ICG, heptamethine dyes exhibit greater photothermal efficiencies. However, they typically possess limited aqueous solubility and low photostability. As a general rule, heptamethine dyes exhibit efficient PDT properties. As a result, both PTT and PDT effects can contribute to their *in vivo* activity.

Cheng *et al.* encapsulated a NIR-absorbing heptamethine dye, IR825, within PEGylated micelles to create the putative PTT agent **7** (Fig. 2B).[12] Solutions of **7** (0.5 mg/mL) in water showed a temperature enhancement (ΔT = ~45 °C) upon irradiation (5 min, 808 nm laser, 0.5 W/cm^2). Administration of **7** (1 mg/mL, 200 μL) *via* intravenous injection in 4T1 tumor-bearing mice, followed by irradiation (5 min, 808 nm laser, 0.5 W/cm^2) resulted in a temperature increase that exceeded 60 °C. As importantly, effective tumor reduction was seen without significant side effects in these animal models.

The dye IR780 was used by Yue *et al.* to create the heparin-folic acid system **8** (Fig. 2C). This construct, designed to achieve cancer targeting, was found to absorb NIR light strongly with a maximum at ~780 nm. It was also found to emit at ~807 nm.[13] A suspension containing 10 μg/mL of **8** in water produced a clear increase in temperature upon irradiation (by ~19 °C from 23 °C, 2 min, 808 nm laser, 0.6 W/cm^2). Excellent photothermal stability

was seen under these conditions. When injected intravenously at a dose of 1.4 mg/kg, construct **8** induced significant tumor size reduction following photoirradiation (5 min, 808 nm laser, 0.8 W/cm^2) in folate receptor-positive MCF-7 tumor xenografts.

Luo *et al.* investigated a library of heptamethine dyes and found that dye **9** (Fig. 2D) produced good PTT and PDT effects and displayed excellent mitochondrial targeting.[14] Compound **9** gave rise to a temperature increase of ~28 °C from 28 °C when irradiated in methanol (2 min, 808 nm laser, 1.5 W/cm^2). It also produced ROS effectively and outperformed other related compounds, as well as ICG itself. The mitochondria are particularly sensitive to both PTT and PDT. Therefore, it is perhaps not surprising that **9** gave rise to demonstrable phototoxicity in four cancer cell lines (A549, H460, 4T1, and MCF-7), as well as in 4T1 tumor xenografts.

The heptamethine dye **10** (Fig. 2E) is of interest. It undergoes pH-dependent switching between a PTT active neutral and a fluorescent cationic state. In the neutral state, an intramolecular charge transfer (ICT) process from the amine serves to quench the fluorescence and promote non-radiative deactivation of the excited singlet state.[15] Upon protonation of the amine, the ICT process is inhibited, resulting in NIR fluorescent emission. In slightly basic media (pH 7.4), a 10 μM solution of **10** gave rise to a temperature increase of ~ 37 °C from an initial value of 25 °C when subject to irradiation (2 min, 750 nm laser, 6.0 W/cm^2). In contrast, an analogous acidic solution (pH 2.4) not containing **10** resulted in an increase of less than 10 °C under otherwise identical irradiation conditions. In both HepG2 and HeLa cells, probe **10** (20 μM) was found to produce a detectable fluorescence emission within the acidic lysosomes, which were 2.8 and 2.7 times higher than that of normal HL-7702 cells. Significant cytotoxicity in both HepG2 (82.8%) and HeLa (84.8%) cells was also observed after photoirradiation (10 min, 750 nm laser, 6.0 W/cm^2). These findings are ascribe to the efficiency of **10** as a PTT agent within the alkaline mitochondrial matrix.

3.3. Phthalocyanine-based agents

Phthalocyanines (Fig. 3A) have outstanding optical and thermal stabilities. They also have high molar absorptivities ($\varepsilon > 10^5$ M^{-1}cm^{-1}) in the NIR region.[16] Due to their hydrophobic and planar nature, this class of dyes is prone to aggregate in solution. This results in a reduction in the inherent fluorescence and limits their ability to produce ROS following photoactivation. This makes them less effective as PDT photosensitizers. On the other hand, aggregation favors non-radiative, heat-producing de-excitation pathways, which is desirable for PTT. The fluorescence and ROS-dependent PDT features can be restored by inhibiting aggregation.

In 2009, two metallonaphthalocyanines, containing coordinated Pd(II) and Pt(II) ions, respectively, were developed and characterized (Fig. 3A).[17] These complexes were found to possess good photothermal features while producing very low levels of ROS, as inferred from both cell studies involving the B78H1 amelanotic melanoma cell line and subcutaneously transplanted tumor mice models. The PTT effects were rationalized in terms of a shortened triplet lifetime of the metallonaphthalocyanines resulting from their being aggregated within specific subcellular compartments.

Mathew *et al.* reported another example of a napthalocyanine-based formulation (**11**) that provides near-exclusive temperature increases upon irradiation.[18] The system in question consists of a gadolinium-bisnapthalocyanine sandwich complex (GdSand) (Fig. 3B) encapsulated in a high-density lipoprotein (HDL). This formulation produces aggregates that could be further functionalized with a cell-penetrating TAT peptide to produce **11**. A toluene solution containing nanoparticles **11** (0.33 μM, GdSand) gave rise to a temperature increase of ~7 °C from 37 °C with no significant singlet oxygen production under 770 nm laser irradiation (3 min, 1.5 W). Cellular uptake, presumed to be Tat-mediated, and *in vitro* photothermal therapy were demonstrated in NCI-H460 cells.

Tetra-*t*-butylphthalocyanine ($PcBu_4$) has been used to produce aggregates **12** stabilized by polymeric encapsulation (Fig. 3C). The resulting system produced significant benefits as compared to solutions of $PcBu_4$ or non-stabilized aggregates. With **12**, an increase of ~32 °C from 25 °C in water (3 min, 671 nm, 6.4 W/cm^2) was achieved.[19] These nanoparticles demonstrated efficient tumor accumulation, an effect ascribed to their appropriate size (~60 nm), as well as effective PTT in a SCC7 cell-bearing mice model.

As noted above, the PDT features of phthalocyanines can be restored in part by inhibiting aggregation. Wei *et al.* described a nanoparticle system (**13**) with both PDT and PTT capabilities. The nanoparticles in question consisted of silicon 2,3-naphthalocyanine dihydroxide (SiNcOH) encapsulated in an amphiphilic PEGylated phospholipid (Fig. 3D).[20] A 150 ppm aqueous mixture of nanoparticles **13** produced a significant temperature increase of ~26.7 °C from an initial temperature of 26 °C while generating singlet oxygen upon irradiation (12 min, 808 nm laser, 1.5 W/cm^2). System **13** was found to act as a theranostic agent in that it permitted photoacoustic (PA) imaging in a HeLa xenograft mouse model. Its utility as a PTT agent was supported by the demonstration of efficient tumor eradication in this model upon 808 nm NIR laser irradiation. These therapeutic benefits were rationalized in terms of a combined PTT and PDT effect.

Another dual PDT/PTT system (**14**) was reported by Taratula *et al.*.[21] In this case, silicon 2,3-naphthalocyanine bis(trihexylsilyloxide) (SiNc2) was encapsulated into polypropylenimine dendrimer micelles that were further decorated with PEG moieties (Fig. 3E). System **14** was designed such that within the nanoparticles the SiNc2 would be partially solvated and thus not fully aggregated. This was expected to allow for fluorescence monitoring and PDT effects that could complement those involving PTT. Per the design expectations, aqueous mixtures of **14** (100 μg/mL) displayed both PDT and PTT effects under 785 nm laser irradiation (5 min, 1.3 W/cm^2). Under these conditions, a temperature increase of ~39 °C (from 25 °C) was recorded and good photo- and thermal stabilities were observed. The potential utility of the system was demonstrated in drug-resistant A2780/AD ovarian cancer cells and in mice bearing tumor xenografts.

3.4. Other cyanine-based agents

Zhou *et al.*, have helped broaden the scope of the cyanine class of dyes by developing the hemicyanine-rhodamine hybrid (structure RC in Fig. 4A).[22] In methanolic solution, this cyanine derivative displays a broad absorbance centered at ~868 nm with a shoulder at ~950

nm. Very little fluorescence is seen. The biocompatibility of RC was improved by preparing a RC-bovine serum albumin (BSA) complex. Under conditions of laser irradiation (10 min, 915 nm, 1.0 W/cm^2), RC (0.1 mM) produced a significant temperature enhancement by ~26 °C from 23 °C with a 28.7% photothermal conversion efficiency. It also displayed excellent photostability. In a 4T1 tumor model, the BSA complex **15** exhibited good PTT performance both *in vitro* and *in vivo* without evidence of significant long-term toxicity.

Recently, Kim and coworkers reported a functionalized cryptocyanine derivative **16** for use in PTT.[23] Derivative **16** incorporates triphenylphosphonium (TPP) groups. The charged TPP moieties were designed to serve a double purpose, namely targeting to the mitochondria of cancer cells and preventing excessive aggregation. Sensitizer **16** displays an intense absorption peak at 713 nm and a second weaker absorbance feature at 780 nm in DMSO. Upon laser irradiation (5 min, 730 nm, 3.0 W/cm^2), a solution of **16** showed good temperature enhancement (ΔT = 24.5 °C) with a 9.5% photothermal conversion efficiency with little evidence of ROS production. Per the design expectations, **16** was found to localize well in the mitochondria of HeLa cells and display efficient cytotoxicity under conditions of photoirradiation.

4. Diketopyrrolopyrrole-based agents

Owing to their high molecular absorption coefficients and excellent photostability, as well as absorbance features that can be shifted into the NIR region, diketopyrrolopyrroles have been used extensively as chromophores in the development of PTT agents. In solution, isolated diketopyrrolopyrroles tend to display relatively high fluorescence quantum yields; however, this fluorescence is efficiently quenched under conditions of self-aggregation. Thus, in self-assembled colloidal solutions, diketopyrrolopyrroles are excellent PTT-active agents that are typically characterized by very high photothermal yields. This is particularly true when incorporated as the electron deficient component into fused donor-acceptor-donor (D-A-D) systems.

The group of Xiaochen Dong reported the use of *NN,* -diphenyl-4-(2-thienyl)aniline substituents as the electron donor groups in diketopyrrolopyrrole-containing D-A-D systems, an approach that produced conjugates with strong NIR absorbance.[24] The D-A-D construct in question (DPP-TPA) relies on an electron rich aromatic amine to complement the electron deficient diketopyrrolopyrrole core. Reprecipitation of a THF solution of DPP-TPA into water yielded monodisperse aggregates (**17**) with an average size of 76 nm (Fig. 5B). Upon excitation (10 min, 660 nm laser, 1 W/cm^2), a PBS solution containing 80 μg/mL of **17** gave rise to a rapid increase in the temperature (by ~35 °C starting from 25 °C), whereas a control PBS solution showed only a marginal increase. Nanoparticles **17** were found to exhibit a photothermal conversion efficiency of 34.5%, as well as a singlet oxygen generation efficiency of 33.6%. In a murine cancer xenograft model subject first to intravenous injection with nanoparticles **17** (0.2 mg/kg) and then irradiation (660 nm laser, 1 W/cm^2 at the tumor site), a significantly increased intratumoral temperature was observed. Full tumor eradication was demonstrated two days after the initiation of the treatment, presumably due to the combined effect of PDT and PTT.

The same research team reported another small organic molecule diketopyrrolopyrrole (SDPP) that bears 4-(*NN,* -dimethylamino)-4′-(2-thienyl)-substituted benzophenone moieties as the donor groups.[25] These D-A-D systems form cubic nanoparticles (**18**) with an average size of ~123 nm (Fig. 5C). The nanoparticles (40 μg/mL) produce a large increase in solution temperature as compared to SDPP under otherwise identical conditions. When administrated intravenously to tumor bearing mice, nanoparticles **18** (40 μg/mL, 100 μL) give rise to a measurable increase in temperature upon irradiation (660 nm laser, 1 W/cm^2). Moreover, full tumor ablation is seen 8 days subsequent to initiation of the phototherapy regimen.

Pu *et al.* published a series of nanoparticles (**19**–**21**, Fig. 5D) based on alternating D-A semiconducting polymers containing diketopyrrolopyrrole moieties, namely SP2-SP4 (Fig. 5A), as the acceptor groups.[26] These nanoparticles were obtained as monodisperse 46 nm-sized particles *via* nanoprecipitation with DSPE-mPEG$_{2000}$. Among the three constructs obtained in this way, the system based on SP4 (**21**) displayed the smallest bandgap, highest molecular absorbance coefficient on a per weight basis, and the best photothermal conversion efficiency. Nanoparticles **21** (20 μg/mL, PBS pH 7.4) produced a temperature increase of ~23 °C (from 22 °C) upon irradiation (4 min, 808 nm laser, 0.24 W/cm^2).

In separate work, Liu *et al.* synthesized poly(dithienyl-diketopyrrolopyrrole) (PDPP)-containing nanoparticles **22** (Fig. 5E) that incorporate the amphiphilic block co-polymer Pluronic F127.[27] In this case, 50 nm-sized **22** nanoparticles were obtained. When studied at a concentration of 40 ppm, an increase in temperature (ΔT = ~20 °C) (10 min, 808 nm laser, 1.0 W/cm^2) in water was seen. In contrast, analogous irradiation of a blank solution produced only a modest temperature increase (ΔT = ~5 °C) under otherwise identical conditions. Nanoparticles **22** could be loaded with DOX. The release of the encapsulated DOX from the nanoparticles was found to follow a complex temperature dependent relationship. However, importantly, the viability of cells incubated with DOX-loaded nanoparticles **22** was found to be significantly reduced under conditions of NIR irradiation.

5. Croconaine-based agents

The group of B. D. Smith pioneered the use of croconaine dyes for photothermal therapy. These chromophores are attractive for their high photostability and low fluorescence quantum yields, as well as their very short-lived excited state lifetimes.

Croconaine dye(Croc) (Fig. 6A) was studied in chloroform and was found to produce virtually no singlet oxygen.[28] Irradiation of a sample of 4 μg/mL of Croc in chloroform (10 min, 808 nm laser, 3.5 W/cm^2) resulted in a modest temperature increase (ΔT = ~2 °C). The absorbance of the croconaine core could be shifted to the red through formation of a pseudo-rotaxane (CrocRot I) (Fig. 6A). This architecture gave a higher degree of laser light absorption and produced a 5-fold temperature increase (i.e., ΔT = ~10 °C) relative to Croc alone. The related system, CrocRot II (Fig. 6A), was also studied. This latter system displayed not only a bathochromic absorbance versus Croc, but also a 3-fold reduction in the fluorescence quantum yield. Further modifications were made to enhance the water solubility of the croconaine chromophore; this resulted in the preparation of

Bis(guanidinium) Croc (Fig. 6A). Using it, a water-soluble pseudorotaxane structure CrocRot III(Fig. 6A) was prepared. This latter syste, displayed a substantially increased photostability relative to Bis(guanidinium) Crocin water. [29]

Both Dumbbell Croc and the rotaxane CrocRot II (Fig. 6B) were studied in 12 nm-sized silicated Pluronic F127 nanoparticles (**23** and **24**). These nanoparticles displayed efficient photothermal effects, giving rise to temperature increase (ΔT= ~12 °C)upon photoirradiation (20 min, 808 nm laser, 3.5 W/cm^2).[29] Dumbbell Croc was also studied in hybrid core-shell nanoparticles and liposomes, such as **25**.[29] Studies involving **25** served to confirm the virtual absence of singlet oxygen produced by the consitutuent croconaine dye. Nevertheless, a significant temperature increase (ΔT = ~15 °C) in solution upon photoirradiation (15 min, 808 nm laser) was observed without any apparent loss in PTT efficiency over several cycles (Fig. 6F).

Whereas the combined PTT and PDT effect of some of the agents described in this review can have beneficial effects in the context of cancer treatment, the generation of singlet oxygen is not always an advantage. This duality was noted in comparative studies involving DOX-containing nanoparticles constructed using Dumbbell Croc and ICG as the respective photosensitizer (Fig. 6D). In the case of the DOX-loaded nanoparticles containing Dumbbell Croc, photoirradiation led to virtually no photobleaching of the incorporated DOX. Moreover, no PDT effects were seen. This was not the case for corresponding ICG systems, which presumably produce singlet oxygen and other ROS upon photoillumination. The benefits of avoiding photobleaching were further illustrated in Dumbbell Croc-containing liposomes loaded with carboxyfluorescein (Fig. 6E). In this case, irradiation (5 min, 808 nm laser, 6 W/cm^2) resulted in nearly 90% release of carboxyfluorescein from the liposomes and produced an increase (ΔT = ~45 °C) in the solution temperature.[30] Little evidence of photobleaching or PDT effects was seen.

The pH dependence on the PTT effect was studied in CrocRot IV (Fig. 6G).[31] This rotaxane shows a pH-dependent, ratiometric absorbance as a function of the protonation state of the indole groups (*cf.* structure of CrocRot IV (acidic) in Fig. 6A). Upon irradiation of an acidic (pH 5.0) solution of CrocRot IV (3 μM, 15 min, 808 nm laser, 3.5 W/cm^2) a temperature increase (ΔT = ~10 °C) was observed. The corresponding values were ΔT= ~4 °C and ΔT < 1 °C for solutions at pH 6.5 and 7.2, respectively (Fig. 6G).[31] As the extracellular environment surrounding solid tumors is often more acidic than normal tissues, a pathology-specific turn-on behavior could be envisioned.

Croconaine dyes and systems that contain them have provided important insights that may guide future developments. However, it is important to note that in comparison with other types of PTT agents, croconaine dyes require significantly higher laser power to achieve effective photoirradiation. Also, relatively modest temperature increases are observed. Finally, a *bona fide* PTT effect *in vivo* has yet to be demonstrated.

6. Porphyrin-based agents

In solution, non-aggregated free-base porphyrins typically give rise to two types of absorbance features in the visible portion of the electronic spectrum: The so-called Soret band, a very intense hypsochromic absorbance, and four bathochromic Q-bands with relatively low absorbance. In order to improve the photophysical properties of porphyrins for applications as *in vivo* PTT agents, the excited-state lifetimes need to be shortened. This can be achieved by promoting self-assembly (i.e. forcing aggregation) within nano-objects, or through the complexation of certain metal cations within the porphyrin core, or both. In this section we summarize efforts to modify porphyrins for use in PTT.

Lovell *et al.* described the synthesis of porphysomes (e.g., **27**), 100 nm-sized liposome-like structures formed from the self-assembly of a modified phospholipid. In these systems, referred to as phosphatidylcholine-pyropheophorbides, one phospholipid fatty acid chain was replaced by a pyropheophorbide, a porphyrin analogue of natural origin (Fig. 7A–B).[32] The stability and *in vivo* pharmacokinetics were further improved by the addition of 5% mPEG-DSPE. With this modification, the fluorescence was found to be reduced almost 1,600-fold relative to the free pyropheophorbide. Presumably as the result of using compounds of natural origin, the porphysomes **27** proved to be fully biodegradable. These nanoparticles were well tolerated by mice at doses up to 1g/kg. This tolerance was reflected in blood chemistries that were essentially within the normal range during the two week monitoring period that followed porphysomes administration. In a formulation containing an additional 30% cholesterol, 42 mg/kg of these porphysomes were injected into tumor-nearing mice and the photothermal effect was studied. An increase in the temperature by 30 °C was seen within the tumor region upon irradiation (1 min, 658 nm laser, 1.9 W/cm^2).

Using a similar porphysome formulation, the authors studied the relative contribution of PDT to the efficacy of cancer therapy of the porphysomes by making comparisons to Photofrin, a clinically approved PDT agent. Two xenograft tumors were transplanted in the left and right flanks of mice. One tumor was photoilluminated while the animals were maintained in a 100% oxygen environment. The other tumors were treated in a chamber containing 7% oxygen with the blood supply to the tumor being restricted *via* a tourniquet. Under conditions of photoillumination (dose 100 J/cm^2, power: 200 mW), Photofrin resulted in the clear eradication of the tumor under hyperoxic, but not hypoxic conditions. Porphysomes did not demonstrate any significant tumor growth reduction under either of these two conditions, and the tumor temperature was elevated by less than 5 °C. However, when treated using the same total light dose but at a higher irradiation power (dose 100 J/cm^2, power: 750 mW) the tumors were eradicated from both the hypoxic and hyperoxic tumors.[33] This duality of action was ascribed to a PTT effect.

Zhou *et al.* described a tetraphenylporphyrin conjugate (TPP-G-FF) bearing a short linker and the phenylalanine-phenylalanine dipeptide **28** (Fig. 7D).[34] Upon reprecipitation in water, aggregates were obtained, the size of which could be tuned to 25 ± 10 nm. The structure of the aggregates and the driving force for their self-assembly was studied *via* molecular dynamics; this revealed a major contribution from hydrophobic J-type π-π interactions of the tetraphenylporphyrin core, as well as hydrogen bridges between the phenylalanine

subunits and the surrounding water molecules. Upon irradiation of a sample of **28** (10 min, 635 nm laser, 1.2 W/cm^2) a temperature increase of 35 °C (from 25 °C) with a 54.2% photothermal conversion efficiency was observed. Under these conditions, essentially total quenching of the fluorescence and near-complete repression of singlet oxygen production was seen. *In vivo* studies in tumor-bearing mice revealed a tumor-site temperature increase to 58 °C after irradiation for 10 min. Eradication of the tumor was also seen.[34]

Inducing a bathochromic shift in the low energy absorbance features of the porphyrins used for PTT would be highly advantageous since it would allow irradiation in spectral regions where bodily tissues are most transparent. Guo *et al.* achieved this goal *via* the incorporation of a porphyrin subunit into an alternating D-A type conjugated polymer (PorCP).[35] In PorCP, the lowest energy absorbance band is redshifted to 815 nm. The polymers were reprecipitated in the presence of DSPE-PEG$_{2000}$-Maleimide to form 40 nm-sized nanoparticles **29**. Further decoration with a short cell-penetration peptide ensured efficient cellular uptake. Irradiating (10 min, 808 nm laser, 0.75 W/cm^2) a 0.1 mg/mL solution of nanoparticles **29** produced a temperature increase of ~52 °C (from 24 °C). A very high photothermal conversion efficiency of 63.8% was found. However, it was also reported that the corresponding irradiation of a blank solution served to increase the temperature by ~15 °C (from 24 °C). This blank value far exceeds that reported by other groups. In spite of this potential dichotomy, a clear irradiation-time dependent reduction in tumor size was seen *in vivo* for nanoparticles **29** using a genetic zebrafish model of liver hyperplasia.[35]

7. Polymer-based agents

Polymeric PTT agents have been recently reviewed by Ban *et al.*[36] Nevertheless, a brief summary is appropriate here since discrete polymers have been used to create nanoparticles with PTT capabilities that provide a complement to stand-alone agents and liposomal constructs. Many of the light absorbing organic polymeric nanomaterials considered in the context of PTT (Fig. 8A) have been extensively studied in nanomedicine particularly as drug/gene delivery carriers, including in the context of clinical trials. This has likely helped accelerate their development for PTT applications.

Yang *et al.* described a set of purple-colored homogeneous nanoparticles **30** (emeralidine base), that are capped with PEGylated fatty acid groups (poly(ethylene glycol)stearate) to improve the aqueous solubility (Fig. 8B).[37] Under acidic conditions (pH = 1), a charge transfer peak originating presumably from interactions between the quinoid and benzenoid rings within the polymer, is seen at 810 nm. In contrast, the lowest energy feature was observed at 580 nm at pH = 7.4. Similar red-shifted absorbance features were seen upon incubating **30** in the presence of oxidants, resulting in the formation of green colored nanoparticles **31**. Irradiation, **31** (0.5 mg/mL) in pure water produced a temperature increase by ~40 °C from 28 °C (3 min, 808 nm laser, 2.45 W/cm^2) under conditions where the temperature of a control solution rose by only 6.6 °C. The ability of **30** to effect *in vitro* photothermal ablation was validated in A431 cells. During the course of incubation, the color of the nanoparticles **30** changed to green with a substantial shift in absorption maximum of the charge transfer band (to 700 nm) being seen. This change was ascribed to the presence of protons and oxidative species. Irradiation with 808 nm laser (5 min, 2.45

W/cm^2) led to eradication of A431 cells incubated with **30**, with corresponding tumor growth inhibition being seen in A431 tumorbearing animal model s.

Cheng *et al.* reported a polymeric 100 nm-sized nanomaterial (**32**) based on poly(3,4-ethylenedioxythiophen):poly(4-styrene-sulfonate) (PEDOT:PSS) that was further coated with PEG, to improve the physiological stability and increase the blood circulation time (Fig. 8C).[38] Irradiation of **32 (**0.1 mg/mL in water) resulted in a temperature increase of ~35 °C from an initial value of 16 °C (5 min, 808 nm laser, 1 W/cm^2). In 4T1 tumor-bearing mice, a high degree of **32** NP accumulation in tumor was seen at 24 h (16.33% ID/g) and 48 h (28.02% ID/g) post intravenous injection. Upon photoirradiation (5 min, 808 nm laser, 0.5 W/cm^2), essentially complete tumor regression was seen.

In another report, Yang *et al.* disclosed a set of polyvinyl alcohol(PVA) -stabilized polypyrrole (PPy) nanoparticles (**33**) prepared *via* a microemulsion approach (Fig. 8D).[39] In aqueous solution these nanoparticles engendered a concentration-dependent temperature rise upon irradiation at 808 nm, while a strong PTT response was seen *in vitro* across a number of cancer cell lines (5 min, 808 nm laser, 0.5 W/cm^2). The *in vivo* therapeutic efficacy of these PPy nanoparticles was tested in 4T1 tumor-bearing female Balb/c mice. In these studies, **33** was administrated intravenously (dose = 2 mg/kg) before the tumors were exposed to 808 nm laser at different power levels (*i.e.,* 0.1, 0.25, 0.5 W/cm^2) for 5 min. Tumors treated with PPy **33** and irradiated with a laser power of 0.5 W/cm^2 were completely ablated. No evidence of tumor reoccurrence was seen. No such beneficial effects were seen in the case of the controls(i.e., PPy or light alone).

A multimodal theranostic agent was developed by coating supermagnetic iron oxide nanoparticles (SPION) with PPy and further decorating with an amphiphilic bloc-copolymer (C18PMH-PEG). The resulting nanoparticles were finally loaded with DOX to give **34** (Fig. 8E).[40] In the absence of light, these nanoparticles showed pH-dependent DOX release behavior with the greatest release being observed at pH 5.0. Irradiation (808 nm laser, 5 min, 0.75 W/cm^2) further enhanced DOX release, presumablyas the result of a weakening of the ionic interactions between the embedded drug and the polymeric chains. The cell viability of 4T1 cancer cells was reduced by 90% after incubation with **34** and double activation (placing in a magnetic field and subjecting to NIR laser irradiation). This reduction proved significantly higher than what was seen under conditions of single activation (35% and 50% in the case of an applied magnetic field and NIR illumination, respectively). The *in vivo* therapeutic efficacy of **34** was validated in 4T1 tumor-bearing mice models under conditions of 808 nm laser irradiation (25 min, 0.35 W/cm^2). Mice treated with Fe_3O_4@PPy-PEG-DOX (8 mg/kg) exhibited 88% tumor growth inhibition as compared to control groups [50% for DOX (1 mg/kg) + laser illumination; 30% for Fe_3O_4@PPy-PEG (8 mg/kg) + laser illumination; 50% for Fe_3O_4@PPy-PEG-DOX (8 mg/kg) in the absence of illumination]. The therapeutic efficacy of **34** could be followed using by T2-weighted magnetic resonance imaging. This latter monitoring reflects, presumably, the fact that the SPION making up **34** are excellent T2 contrast agents.

In 2013, Zha *et al.* synthesized uniformly sized PPy nanoparticles (~46 nm) by a simple onestep aqueous dispersion polymerization method using PVA as a stabilizer (Fig. 8F, top

line).[41] Compared to Au nanorods capped with cetyltrimethylammonium bromide (CTAB), these PPy nanoparticles showed excellent photothermal conversion efficiencies upon NIR light irradiation (10 min, 808 nm laser, 2 W/cm^2). Following cooling, the PTT process could be repeated for up to 5 cycles with no apparent loss of photothermal efficacy. In HeLa cells, both a concentration-dependent and irradiation time-dependent toxicity was observed under conditions of photoillumination (808 nm laser, 6 W/cm^2).

Iron(III) cation-induced oxidative polymerization of pyrroles can lead to the presence of residual Fe^{3+} and Fe^{2+} cations. Tian *et al.* exploited the presence of the latter ions to form *in situ* Fe_2O_3 crystals on the surface of 70 nm sized PPys.[42] The PP y@Fe_2O_3 nanoparticles obtained in this way were studied for their ability to support photothermal imaging, MRI contrast enhancement, and photothermal conversion. It was found that PPy@Fe_2O_3 exhibits an intense and broad absorption band in the NIR region and that irradiation of aqueous dispersions containing PPy@Fe_2O_3 (5 min, 808 nm laser, 0.25 W/cm^2) increased the solution temperature by ~33.5 °C (from an initial value of 22 °C). A 39.15% overall photothermal conversion efficiency was recorded. The PTT effects were found to be concentration-dependent. The PPy@Fe_2O_3 polymeric particles exhibited good photostability (through up to 8 cycles of NIR irradiation). The therapeutic efficacy was further tested in SW-1990 pancreatic cancer cell inoculated xenograft models. When irradiated for a relatively short time with 808 nm NIR laser light of ultra low power density (0.25 W/cm^2, 5 min), nanoparticles PPy@ Fe_2O_3 (100 uL, 0.25 mg/mL) displayed improved therapeutic efficacy as compared with other controls (PBS, PPy@ Fe_2O_3 without light)in these cancer models.

Song *et al.* described an alternative approach to preparing composite materials of interest in the context of PTT. This was done by coating PPy over ultra-small iron oxide nanoparticles (USPION) to provide a magnetic, NIR absorbing composite (**35**, Fig. 8F).[43] The resulting 100 nm-sized USPION@PPy-PEG nanoparticles showed high stability in biological milieus with no significant toxicity being observed in 4T1 and U937 cells *in vitro* (48 h). However, upon irradiation (5 min, 808 nm laser, 1 W/cm^2), the viability of 4T1 cells was found to be reduced in a concentration dependent manner (i.e., to 30% with 50 μg/mL and 18% with 100 μg/mL). By exploiting both the optical and magnetic properties of **35**, *in vivo* photoacoustic and MRI imaging could be successfully performed. The *in vivo* photothermal therapeutic potential of **35** (administered *via* i.v. injection) was tested in 4T1 tumor bearing mice. 24 Hours post injection, the tumor region was illuminated (5 min, 808 nm laser, 1.5 W/cm^2); full eradication of the tumor was seen.

In another report, Zhu *et al.* described the therapeutic potential of PPy-based multifunctional composite/hybrid materials for cancer treatment.[44] The inner core of the 100 nm-sized core-shell PPy nanoparticles (**36**, Fig. 8G) consisted of PPy, whereas the shell consisted of a DOX loaded mesoporous MOF (metal-organic framework). Construct **36** (100 μg/mL) in aqueous solution produced an increase in temperature up to ΔT = ~33.8 °C upon photoirradiation (5 min, 808 nm laser, 2 W/cm^2). After loading with DOX the potential of **36** to effect combined drug delivery and PTT treatment was explored. The therapeutic efficacy of PPy@MIL-100 was further tested in HeLa cells with no significant cell toxicity being seen in the absence of illumination up to the 300 μg/mL concentration level. However, both dose- and NIR

irradiation-dependent toxicities were observed in HeLa cells, where 23% cell viability was seen post-treatment (300 μg/mL PPy@MIL-100-DOX (**36**), 5 min, 808 nm laser, 1 W/cm^2). The corresponding nanoparticles without irradiation showed 38% cell viability under the same conditions.

Zhang *et al.* recently reported a proof-of-concept study where pyrene-appended temperature sensitive linkers (pyrene-oxabicycloheptene-alkyne, POA) were attached to the surface of a PPy containing polymeric particle via a copper(I)-catalyzed alkyne-azide cycloaddition "click-reaction" (**37**, Fig. 8H).[45] Upon irradiation (20 min, 808 nm laser, 2 W/cm^2) of an aqueous solution containing 48 μg/mL of **37** a temperature increase of ~50 °C (from 22 °C) was seen; however, a control solution showed a temperature increase of ~35–40 °C under analogous conditions. Upon irradiation for 60 min, a maximum of 89% pyrene release was seen, a result ascribed to temperature-dependent POA fragmentation.

Recently, Yang *et al.* described a nanoparticle **38** based on D-A conjugated polymer poly(BIBDF-BT) (Fig. 8I) with a small bandgap.[46] These 90 nm sized nanoparticles were characterized by a strong absorbance in the NIR spectral region (λ_{max} = 782 nm) and were found to exhibit a 10% singlet oxygen quantum yield. Irradiation (5 min, 785 nm laser, 1.5 W/cm^2) revealed a concentration dependent temperature rise, with an increase (ΔT = ~65.2 °C) within 5 min being seen for a sample containing 20 μg/mL **38**. Compared to Au nanorods or ICG (used as positive controls), not only did **38** show an enhanced photothermal conversion efficiency (34.7%), but also an increased photothermal stability. When administrated intravenously, **38** (1.5 mg/kg) showed preferential tumor accumulation in 4T1 tumor-bearing mice models. When irradiated 24 h post injection at the tumor region (3 min, 758 nm laser, 1.5 W/cm^2) a localized temperature increase (ΔT = ~22 °C) was seen concurrent with complete eradication of the tumor.

8. Other agents

One of the problems associated with the use of synthetic photothermal agents is the possibility of long-term toxicity. In an effort to overcome this potential limitation, Liu *et al.* studied colloidal nanospheres (CNSs) obtained via the oxidation and self-polymerization of endogenous dopamine.[47] The resulting 70 nm-sized melanin-dopamine CNSs demonstrated a broad absorbance spanning the entire visible spectrum and reaching into the NIR. Upon irradiation of a suspension of 200 μg/mL melanin-dopamine CNSsin water (8 min, 808 nm laser, 2 W/cm^2), the temperature was found to increase by ~33.6 °C (from 25 °C) (Fig. 9B). The *in vivo* applicability of these presumably highly biocompatible CNSs was demonstrated in 4T1 tumor-bearing mice. A dramatic reduction in tumor size was seen without any evidence of regrowth after administration and subjecting to NIR irradiation (5 min, 808 nm laser, 2 W/cm^2). The authors demonstrated that their CNSs could undergo post-synthetic modification, as exemplified by their conjugation to Gd-DTPA. The resulting constructs displayed clear tumor accumulation after intravenous injection, as inferred from MR imaging.

Squaraine dyes exhibit bright NIR fluorescence, high absorbance coefficients and desirable photostability. However, their intrinsic chemical instability as well as their propensity to

undergo self-aggregation in aqueous media has limited their utility in PTT applications. To overcome this limitation, Gao *et al.* developed a nontoxic squaraine dye construct *via* association with a natural carrier protein, bovine serum albumin (SQ-BSA, Fig. 9C).[48] Due to aggregation, free squaraines exhibit minimal fluorescence in aqueous media. However, treatment with BSA results in the formation of a fluorescent SQ-BSA adduct. For active tumor targeting application, SQ-BSA was conjugated with folic acid (FA). The potential utility of SQ-BSA-FA to effect *in vivo* tumor imaging and therapy was studied using a KB xenograft mouse model. Good tumor targeting and retention in the tumor region was observed 4 h post injection. Irradiation of the tumor region (30 min, 680 nm laser, 20 W/cm^2, 2-day interval for 16 days) resulted in 78% tumor growth inhibition.

In another report, Huang *et al.* detailed the development of a small molecule-based dye, benzo[1,2-c;4,5-c′]bis[1,2,5]thiadiazole-4,7-bis(5-(2-ethylhexyl)thiophene) (BBTEHT), which the authors suggested could act as a potential alternative to gold nanorods in the context of PTT.[49] When this hydrophobic chromophore was encapsulated by Pluronic 127, nanoparticles **39** were obtained (Fig. 9D). These constructs were evaluated for their photothermal efficiency alongside commercially available gold nanorods. Irradiation of aqueous media containing **39** or Au nanorods (35 μg/mL, respectively) (20 min, 808 nm laser, 1.77 W/cm^2) resulted in temperature increases of up to 42.0 °C and 43.6 °C, respectively. Studies of PTT involving irradiation of **39** in caki-2 cell lines (20 min, 808 nm laser, 1.77 W/cm^2) revealed a 40% reduction in cell viability. Increasing the irradiation time to 20 min, produced 100% cell death, with comparable results being seen for the gold nanorods.

A different PTT strategy was recently reported by Jiao *et al.* These researcher used a supramolecular host-guest strategy to create a 1:2 bola-type amphiphilic perylene diimide (BPDI) complex with cucurbit[7]uril (*i.e.,* BPDI/($CB[7]_2$), Fig. 9E).[50] As a result of the complexation by CB[7], the perylene diimide radical anion is stabilized. Under reductive conditions, the BPDI/($CB[7]_2$) radical anion exhibits a strong photothermal effect. Under conditions of photoillumination (0.3 mM BPDI/($CB[7]_2$), 10 min, 808 nm, 1 W/cm^2), a temperature increase of ~19.5 °C (from 25 °C) with an associated photothermal efficiency of 31.6% was seen in aqueous media. While the complex clearly outperformed either BPDI or a blank solution, this appealing approach has yet to be validated *in vitro*.

9. Concluding remarks

In recent years the field of organic molecule-based photothermal agents has advanced considerably. A number of structures, including cyanines, diketopyrrolopyrroles, croconaines, porphyrins, polymers, and others have been found to produce good photothermal effects. Compared to inorganic materials, which have been more widely studied for PTT applications, organic agents have good biodegradability and ease of renal clearance. Moreover, organic PTT sensitizers offer advantages in terms of reproducibility, controlling the preparation, and ease of synthetic modification. It is thus suggested that PTT agents based on organic molecules and materials will emerge as having a key role to play in developing novel cancer therapies with potential clinical utility.

NIR absorbing organic agents with a low fluorescence quantum yield (FL-QY) as well as low singlet oxygen generation yield (SO-QY) can trigger efficient thermal events under conditions of NIR illumination. Among the agents discussed in this review, only ICG has been approved by the US FDA for clinical, albeit in the context of bio-imaging rather than PTT. However, this approval has made it a workhorse agent in the context of PTT research. Currently, increasing attention is being devoted to heptamethines, such as IR825, IR780, IR808, and IR2, and conductive polymers with conjugated structures, on account of their superior photothermal efficiencies and photo-stability relative to ICG. Croconaine dyes have also been studied; they have provided important insights that may guide future developments. However, further work will be needed to obviate concerns, such as the need for higher laser power levels relative to other dye classes and uncertainty about their bioavailability. Other dyes and polymers are at an even earlier stage of development.

Overall, considerable progress has been made in terms of improving the potential of organic PTT agents through a range of strategies, including increased tumor targeting, complementary drug delivery, stimuli-activated heat production and thermally-induced endogenous ROS generation. Furthermore, multimodal approaches are being studied with the goal of combining PTT with photo-acoustic imaging, NIR fluorescence imaging, or MRI.

Since they rely on different non-fluorescent excited state relaxation pathways that can operate in parallel, the combination of PTT and PDT is particularly attractive. PTT, in contrast to PDT, is not directly dependent on intracellular oxygen tension. In fact, because PTT does not rely on the production of singlet oxygen and other ROS, it is potentially effective in hypoxic tumors. On the other hand, PDT typically induces cell death via singlet oxygen and ROS and thus is most effective in highly oxygenated tissues. Sensitizers for both modalities should absorb in the NIR to allow for good light penetration. Where this latter condition is met, systems that combine PTT and PDT have the potential to overcome drug resistance and metastasis.

The field of organic sensitizer-based photothermal agents is relatively young and despite the progress recorded in the recent literature, a number of hurdles need to be overcome in order to translate current developments into clinical practice. Likely more detailed mechanistic studies and efforts to maximize the PTT efficacy and cellular susceptibility to heat will be needed. Further progress in terms of optimizing the delivery of PTT agents to appropriate tissues and the most sensitive subcellular compartments is also likely needed to advance the field. However, appropriately conceived combination strategies, where PTT is used in conjunction with other therapeutic and diagnostic modalities, may allow rapid progress to be made without the need to overcome many of the limitations associated with current PTT agents. We expect that in the coming years, many of these avenues of investigation will be the subject of intensive research effort.

Supplementary Material

Refer to Web version on PubMed Central for supplementary material.

Acknowledgments

This work was supported by CRI project (No. 2009-0081566, JSK) and the Basic Science Research Program (2015R1A6A3A04058789, HSJ and 2017R1D1A1B03032561, PV) from the National Research Foundation of Korea (NRF) funded by the Ministry of Education and the Korea Research Fellowship Program through the National Research Foundation of Korea (NRF) funded by the Ministry of Science and ICT (2016H1D3A1938052, PV). The work in Austin was funded by the National Institutes of Health (CA 686862, JLS) and the Robert A. Welch Foundation (F-0018, JLS).

Notes and references

1. Urano, M., Douple, EB. Thermal effects on cells and tissues. Vol. 1. VSP; Utrecht: 1988. In Hyperthermia and Oncology.
2. Day ES, Morton JG, West JL. J Biomech Eng. 2009; 131:074001. [PubMed: 19640133]
3. Cheng L, Wang C, Feng L, Yang K, Liu Z. Chem Rev. 2014; 114:10869. [PubMed: 25260098]
4. Ng KK, Zheng G. Chem Rev. 2015; 115:11012. [PubMed: 26244706]
5. Zhang S, Xu J, Chen H, Song Z, Wu Y, Dai X, Kong J. Macromol Biosci. 2017; 17:1600258.
6. Duan X, Bai T, Du J, Kong J. J Mater Chem B. 2018; 6:39.
7. Sheng, Z., Zheng, M., Cai, L. Biomedical Nanomaterials. Zhao, Y., Shen, Y., editors. Wiley-VCH Verlag GmbH & Co. KGaA; Weinheim, Germany: 2016. p. 177-206.
8. Yoon H-J, Lee H-S, Lim J-Y, Park J-H. ACS Appl Mater Interfaces. 2017; 9:5683. [PubMed: 28152314]
9. Zheng X, Xing D, Zhou F, Wu B, Chen WR. Mol Pharmaceutics. 2011; 8:447.
10. Chen Z, Zhao P, Luo Z, Zheng M, Tian H, Gong P, Gao G, Pan H, Liu L, Ma A, Cui H, Ma Y, Cai L. ACS Nano. 2016; 10:10049. [PubMed: 27934074]
11. Zheng M, Yue C, Ma Y, Gong P, Zhao P, Zheng C, Sheng Z, Zhang P, Wang Z, Cai L. ACS Nano. 2013; 7:2056. [PubMed: 23413798]
12. Cheng L, He W, Gong H, Wang C, Chen Q, Cheng Z, Liu Z. Adv Funct Mater. 2013; 23:5893.
13. Yue C, Liu P, Zheng M, Zhao P, Wang Y, Ma Y, Cai L. Biomaterials. 2013; 34:6853. [PubMed: 23777910]
14. Luo S, Tan X, Fang S, Wang Y, Liu T, Wang X, Yuan Y, Sun H, Qi Q, Shi C. Adv Funct Mater. 2016; 26:2826.
15. Zhang J, Liu Z, Lian P, Qian J, Li X, Wang L, Fu W, Chen L, Wei X, Li C. Chem Sci. 2016; 7:5995.
16. Gordon, PF., Gregory, P. Organic Chemistry in Colour. Springer-Verlag; Berlin-Heidelberg-London: 1983.
17. Camerin M, Rello-Varona S, Villanueva A, Rodgers MAJ, Jori G. Lasers Surg Med. 2009; 41:665. [PubMed: 19790243]
18. Mathew S, Murakami T, Nakatsuji H, Okamoto H, Morone N, Heuser JE, Hashida M, Imahori H. ACS Nano. 2013; 7:8908. [PubMed: 24053139]
19. Lim C-K, Shin J, Lee Y-D, Kim J, Oh KS, Yuk SH, Jeong SY, Kwon IC, Kim S. Theranostics. 2012; 2:871. [PubMed: 23082099]
20. Wei J-P, Chen X-L, Wang X-Y, Li J-C, Shi S-G, Liu G, Zheng N-F. Chin Chem Lett. 2017; 28:1290.
21. Taratula O, Schumann C, Duong T, Taylor KL, Taratula O. Nanoscale. 2015; 7:3888. [PubMed: 25422147]
22. Zhou B, Li Y, Niu G, Lan M, Jia Q, Liang Q. ACS Appl Mater Interfaces. 2016; 8:29899. [PubMed: 27758099]
23. Jung HS, Lee J-H, Kim K, Koo S, Verwilst P, Sessler JL, Kang C, Kim JS. J Am Chem Soc. 2017; 139:9972. [PubMed: 28644025]
24. Cai Y, Liang P, Tang Q, Yang X, Shi W, Huang W, Zhang Q, Dong X. ACS Nano. 2017; 11:1054. [PubMed: 28033465]

25. Cai Y, Shi W, Tang Q, Liang P, Zhang C, Chen P, Zhang Q, Huang W, Dong X. Nano Res. 2017; 10:794.
26. Pu K, Mei J, Jokerst JV, Hong G, Antaris AL, Chattopadhyay N, Shuhendler AJ, Kurosawa T, Zhou Y, Gambhir SS, Bao Z, Rao J. Adv Mater. 2015; 27:5184. [PubMed: 26247171]
27. Liu H, Wang K, Yang C, Huang S, Wang M. Colloids Surf, B. 2017; 157:398.
28. Spence GT, Hartland GV, Smith BD. Chem Sci. 2013; 4:4240.
29. Spence GT, Lo SS, Ke C, Destecroix H, Davis AP, Hartland GV, Smith BD. Chem Eur J. 2014; 20:12628. [PubMed: 25146580]
30. Guha S, Shaw SK, Spence GT, Roland FM, Smith BD. Langmuir. 2015; 31:7826. [PubMed: 26149326]
31. Guha S, Shaw GK, Mitcham TM, Bouchard RR, Smith BD. Chem Commun. 2016; 52:120.
32. Lovell JF, Jin CS, Huynh E, Jin H, Kim C, Rubinstein JL, Chan WC, Cao W, Hong LV, Zheng G. Nat Mater. 2011; 10:324. [PubMed: 21423187]
33. Jin CS, Lovell JF, Chen J, Zheng G. ACS Nano. 2013; 7:2541. [PubMed: 23394589]
34. Zhou Q, Abbas M, Zhao L, Li S, Shen G, Yan X. J Am Chem Soc. 2017; 139:1921. [PubMed: 28103663]
35. Guo B, Feng G, Manghnani PN, Cai X, Liu J, Wu W, Xu S, Cheng X, Teh C, Liu B. Small. 2016; 12:6243. [PubMed: 27671747]
36. Ban Q, Bai T, Duan X, Kong J. Biomater Sci. 2017; 5:190. [PubMed: 27990534]
37. Yang J, Choi J, Bang D, Kim E, Lim E-K, Park H, Suh J-S, Lee K, Yoo K-H, Kim E-K, Huh Y-M, Haam S. Angew Chem Int Ed. 2011; 50:441.
38. Cheng L, Yang K, Chen Q, Liu Z. ACS Nano. 2012; 6:5605. [PubMed: 22616847]
39. Yang K, Xu H, Cheng L, Sun C, Wang J, Liu Z. Adv Mater. 2012; 24:5586. [PubMed: 22907876]
40. Wang C, Xu H, Liang C, Liu Y, Li Z, Yang G, Cheng L, Li Y, Liu Z. ACS Nano. 2013; 7:6782. [PubMed: 23822176]
41. Zha Z, Yue X, Ren Q, Dai Z. Adv Mater. 2013; 25:777. [PubMed: 23143782]
42. Tian Q, Wang Q, Yao KX, Teng B, Zhang J, Yang S, Han Y. Small. 2014; 10:1063. [PubMed: 24285365]
43. Song X, Gong H, Yin S, Cheng L, Wang C, Li Z, Li Y, Wang X, Liu G, Liu Z. Adv Funct Mater. 2014; 24:1194.
44. Zhu Y-D, Chen S-P, Zhao H, Yang Y, Chen X-Q, Sun J, Fan H-S, Zhang X-D. ACS Appl Mater Interfaces. 2016; 8:34209. [PubMed: 27998104]
45. Zhang H, Xiong L, Liao X, Huang K. Macromol Rapid Commun. 2016; 37:149. [PubMed: 26524109]
46. Yang T, Liu L, Deng Y, Guo Z, Zhang G, Ge Z, Ke H, Chen H. Adv Mater. 2017; 29:1700487.
47. Liu Y, Ai K, Liu J, Deng M, He Y, Lu L. Adv Mater. 2013; 25:1353. [PubMed: 23280690]
48. Gao F-P, Lin Y-X, Li L-L, Liu Y, Mayerhöffer U, Spenst P, Su J-G, Li J-Y, Würthner F, Wang H. Biomaterials. 2014; 35:1004. [PubMed: 24169004]
49. Huang S, Kannadorai RK, Chen Y, Liu Q, Wang M. Chem Commun. 2015; 51:4223.
50. Jiao Y, Liu K, Wang G, Wang Y, Zhang X. Chem Sci. 2015; 6:3975. [PubMed: 29218167]

Biographies

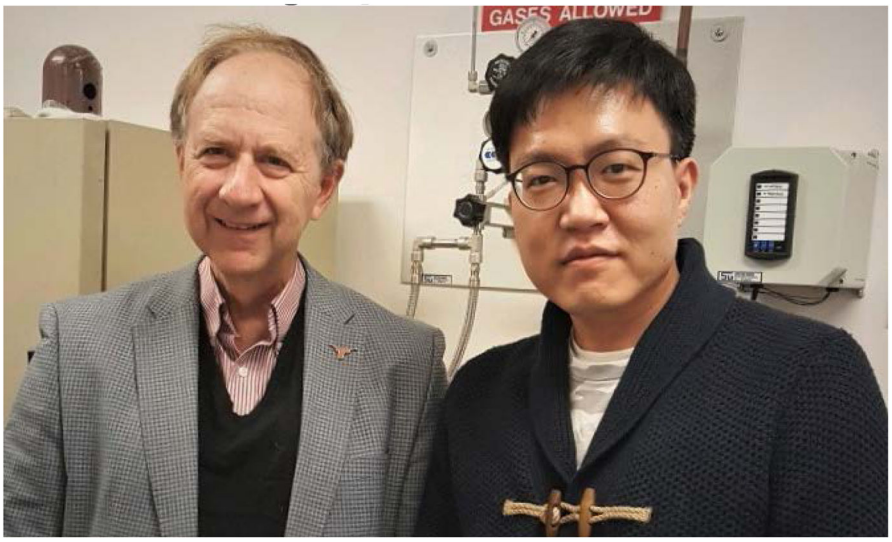

Jonathan L. Sessler (left), Hyo Sung Jung (right)

Hyo Sung Jung received his BS degree in Chemistry from Dankook University and received a PhD degree from Korea University in 2013 under the supervision of Prof. Jong Seung Kim. Since then he has been working as a visiting scholar in Prof. Jonathan L. Sessler's lab at The University of Texas at Austin. He has co-authored 32 scientific publications and is an inventor on 8 patents. His current research interests include targeted theranostic photosensitizers for PDT and PTT and bio-organic sensors.

Prof. Jonathan L. Sessler received a B.S. degree from the University of California, Berkeley and a Ph.D. from Stanford University in 1982 (supervisor: Prof. James P. Collman). He was postdoctoral fellow with first Prof. Jean-Marie Lehn (Strasbourg) and then Prof. Iwao Tabushi's group in Kyoto, Japan. In 1984 he joined the faculty of The University of Texas at Austin, where he is currently the Doherty-Welch Chair. Dr. Sessler has authored or coauthored 680 scientific publications and has 76 issued U.S. Patents. His current Web of Science H-index is 95. Dr. Sessler was a co-founder (with Dr. Richard A. Miller) of Pharmacyclics, Inc., which was acquired by AbbVie for $21B in 2015. Dr. Sessler has recently co-founded Cible, Inc., a new company focused on overcoming cancer drug resistance.

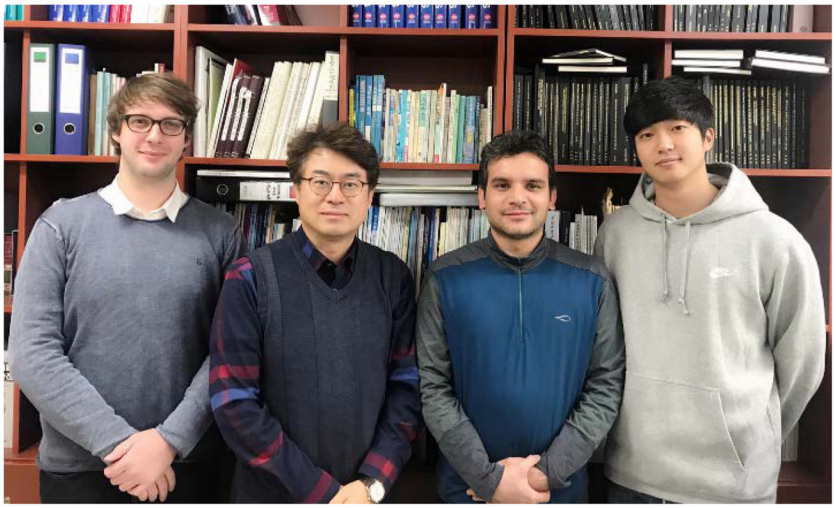

Peter Verwilst, Jong Seung Kim, Amit Sharma, Jinwoo Shin (from left to right)

Peter Verwilst received his Ph. D. from the University of Leuven, Belgium under the supervision of Prof. Wim Dehaen and Prof. Wim M. De Borggraeve in 2011. After a postdoctoral position with Dr. Nathan D. McClenaghan at the Univeristé Bordeaux 1/CNRS, France, he joined the lab of Prof. Jong Seung Kim as a research professor. He has co-authored 35 scientific publications to date and his research interests include theranostic targeted drug delivery and bio-(in)organic sensors.

Amit Sharma received his Ph.D. from Guru Nanak Dev University, Amritsar, India under the supervision of Prof. Kamaljit Singh. He worked in Sphaera Pharma Pvt. Ltd, India as a research scientist (2011–2014). In 2014, he joined Prof. Jong Seung Kim's lab as a research professor. His research interests' center on identifying, understanding, and utilizing mechanisms driving cancer genetic alterations for next generation cancer therapeutics. Outside of the lab, he enjoys hiking, listening to music, and spending time with his family.

Jinwoo Shin received his BS degree from the Department of Chemistry at the Hallym University of Korea in 2015. He is currently pursuing his Ph.D. degree under the guidance of Prof. Jong Seung Kim at Korea University. His current research interests include multimodal theranostic drugs and imaging agents for cancer and Alzheimer's disease.

Prof. Jong Seung Kim received his Ph. D. from the Department of Chemistry and Biochemistry at Texas Tech University in 1993. He spent on year at the University of Houston as a postdoctoral fellow. Currently he is a full professor in the Department of Chemistry at Korea University in Seoul. To date, his research has led to 394 scientific publications (H-index 75) and 80 domestic and international patents. He has been a member of Korea Academy of Science and Technology since 2014.

Key learning points

1. The general concept and importance of organic photothermal therapy (PTT) for cancer.
2. Characteristics of effective organic photothermal agents.
3. Design strategies that are being used to improve the therapeutic efficacy of PTT.
4. Benefits that might accrue from the development of improved organic photothermal agents.
5. Perspectives and considerations that may lead to the development of yet-improved photothermal agents.

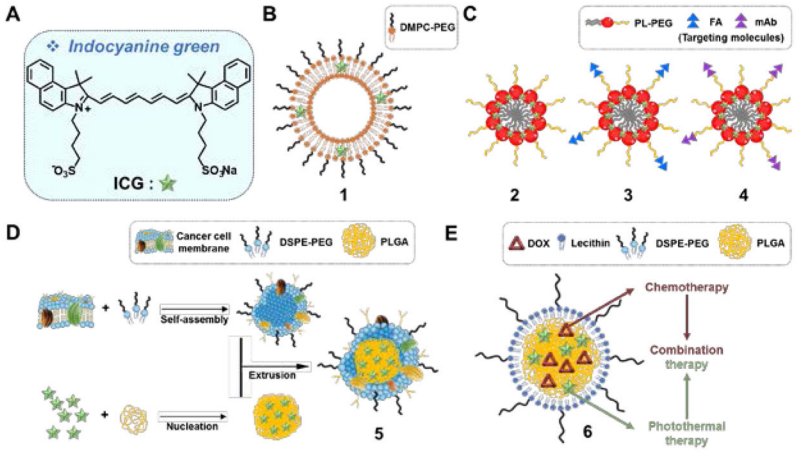

Fig. 1.

(A) Molecular structure of free ICG and its modified forms: (B) ICG/DMPC based liposome **1**, (C) ICG/PL-PEG aggregates **2** conjugated with FA **3** and mAb **4**, (D) ICG/PLGA cancer cell membrane coated biomimetic agent **5**, and (E)ICG/DOX encapsulated lipid-polymer material **6**. DMPC: 1,2-dimyristoyl-*sn*-glycero-3-phosphocholine; PL: phospholipid; PEG: polyethylene glycol; FA: folate receptor; mAb: monoclonal antibody; DSPE=1,2-distearoyl-*sn*-glycero-3-phosphoethanolamine; PLGA: poly(lactic-co-glycolic acid); DOX: doxorubicin.

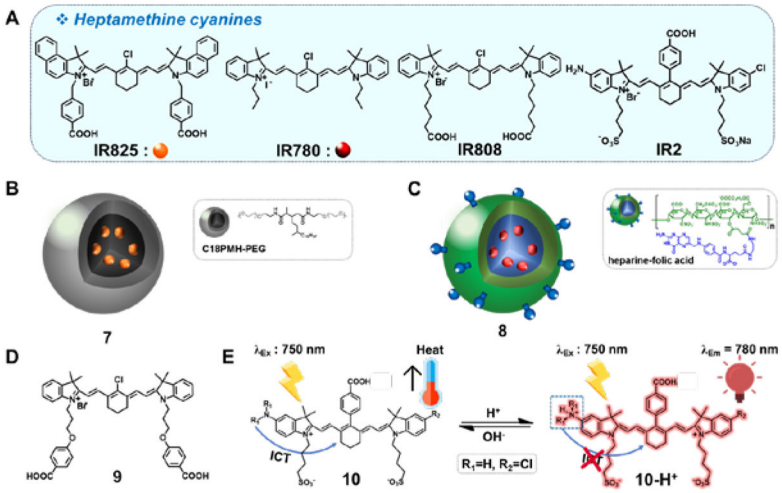

Fig. 2.

(A) Molecular structures of the heptamethine cyanines: IR825, IR780, IR808, and IR2 and associated PTT systems: (B) IR825/PEGylated micelle **7**, (C) IR780/heparine-folic acid system **8**, (D) mitochondria-targetedheptamethine **9,** and (E) pH-switchable theranostic heptamethine dyes**10** and **10-H**$^{+}$.

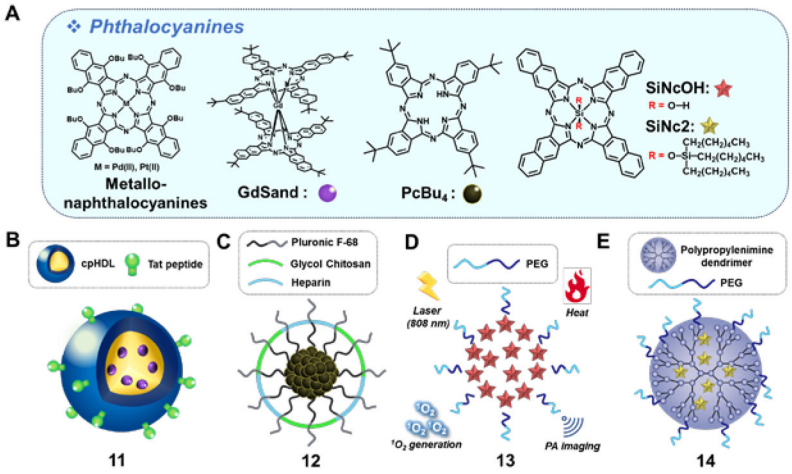

Fig. 3.

(A) Molecular structures of phthalocyanines: metallonaphthalocyanines, GdSand, $PcBu_4$, SiNcOH and SiNc2 and constructs containing these dyes: (B) GdSand/HDL/Tat nanoparticle **11**, (C) $PcBu_4$/Pluronic F-68/glycol chitosan/heparin nanoparticle **12**, (D) PEG-phospholipids encapsulated SiNcOH nanoparticle **13**, and (E) dendrimer-encapsulated SiNc 2 nanoparticle **14**. GdSand: gadolinium-bisnapthalocyanine sandwich complex; $PcBu_4$: tetra-*t*-butylphthalocyanine; HDL: high-density lipoprotein; Tat=transactivator of transcription; SiNcOH: silicon 2,3-naphthalocyanine dihydroxide; SiNc2: silicon 2,3-naphthalocyanine bis(trihexylsilyloxide).

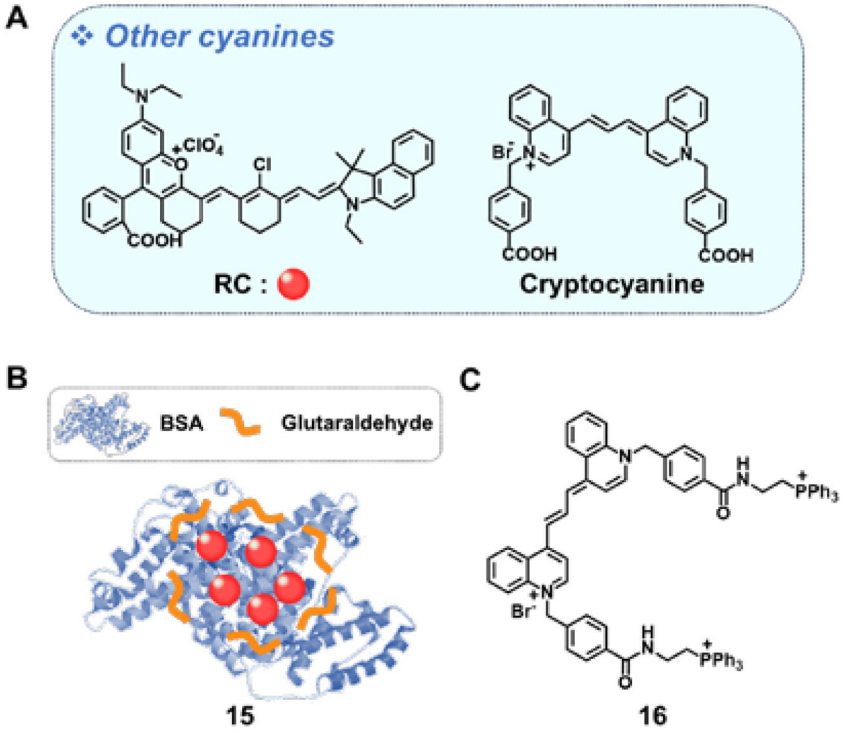

Fig. 4.

(A) Molecular structures of RC and cryptocyanine and constructs prepared from these particular dyes: (B) RC/BSA **15** and (C) TPP-functionalized cryptocyanine **16**. RC: hemicyanine-rhodamine; BSA: bovine serum albumin; TPP:triphenylphosphonium.

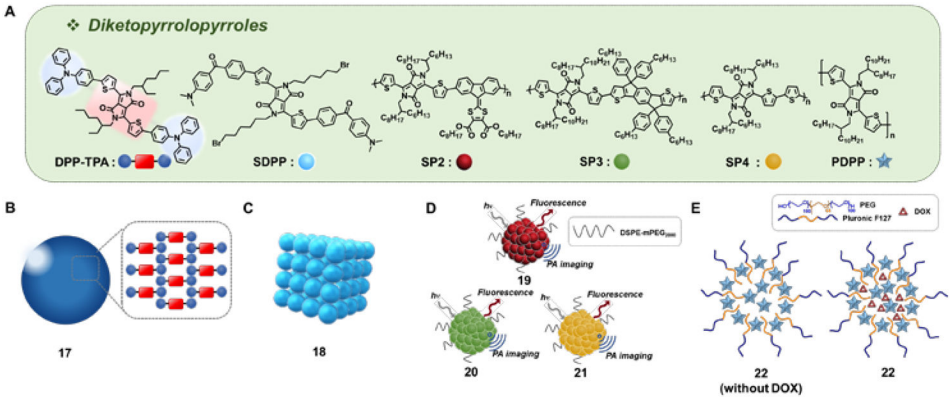

Fig. 5.

(A)Molecular structure of diketopyrrolopyrroles: DPP-TPA, SDPP, SP2, SP3, SP4, and PDPP, and selected derivatives: (B) Diketopyrrolopyrrole triphenylamine nanoparticle **17**, (C) small-molecule diketopyrrolopyrrole-based therapeutic nanoparticles **18**, (D) semiconducting polymeric nanoparticles **19**–**21**, and (E) PDPP-containing nanoparticles **22**. DPP-TPA: dithienyldiketopyrrolopyrrole-triphenylamine; SDPP: 5-bis(6-bromo-hexyl)-3,6-bis[5-[4-(4-dimethylaminobenzoyl)-phenyl]-thiophen-2-yl]-2,5-dihydropyrrolo[3,4-c]pyrrole-1,4-dione; SP: semiconducting polymer; PDPP: poly(dithienyldiketopyrrolopyrrole).

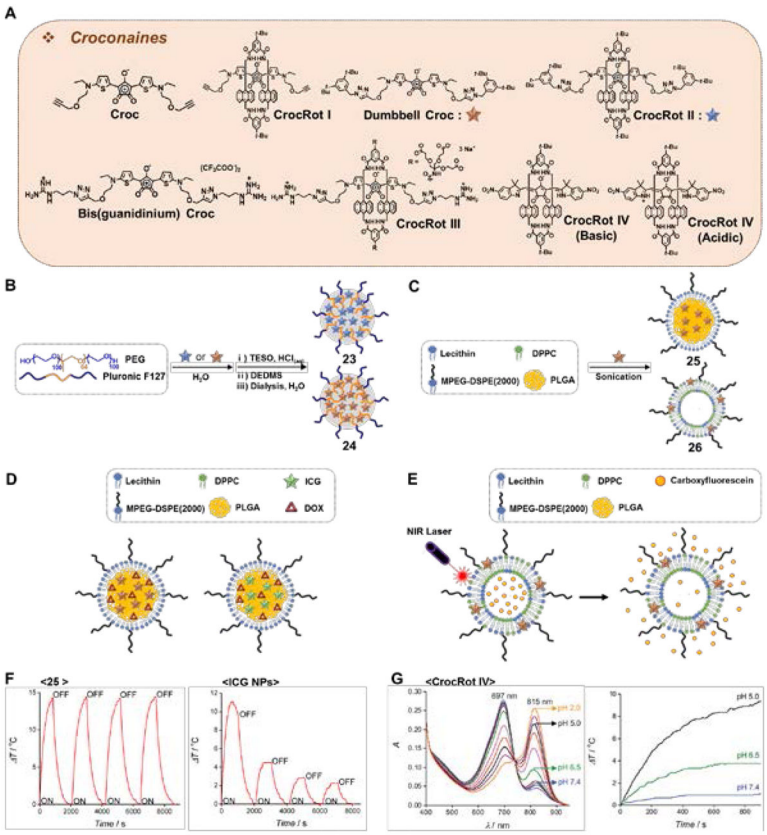

Fig. 6.

(A) Molecular structure of croconaines: Croc, CrocRot I, Dumbbell Croc, CrocRot II, Bis(guanidinium) Croc, CrocRot III, and CrocRot IV. (B) Preparation of Dumbbell Croc-based silicate nanoparticle **23** and CrocRot II-based silicate nanoparticle **24**. (C) Preparation of Dumbbell Croc-based nanoparticles **25** and liposomes **26**, respectively. (D) DOX-containing nanoparticles constructed using Dumbbell Croc and ICG. (E) Dumbbell Croc-containing liposomes loaded with carboxyfluorescein. (F) Unlike ICG, Dumbbell Croc retains its potential to cause a photothermal effect over multiple cycles when incorporated in PLGA/mPEG2000-DSPE nanoparticles **25**. Adapted with permission from Ref. 30. Copyright 2015 American Chemical Society. (G) pH dependent absorbance and PTT effect of CrocRot IV. Adapted from Ref. 31 with permission from The Royal Society of Chemistry. Croc: croconaine dye; CrocRot: pseudorotaxane croconaine.

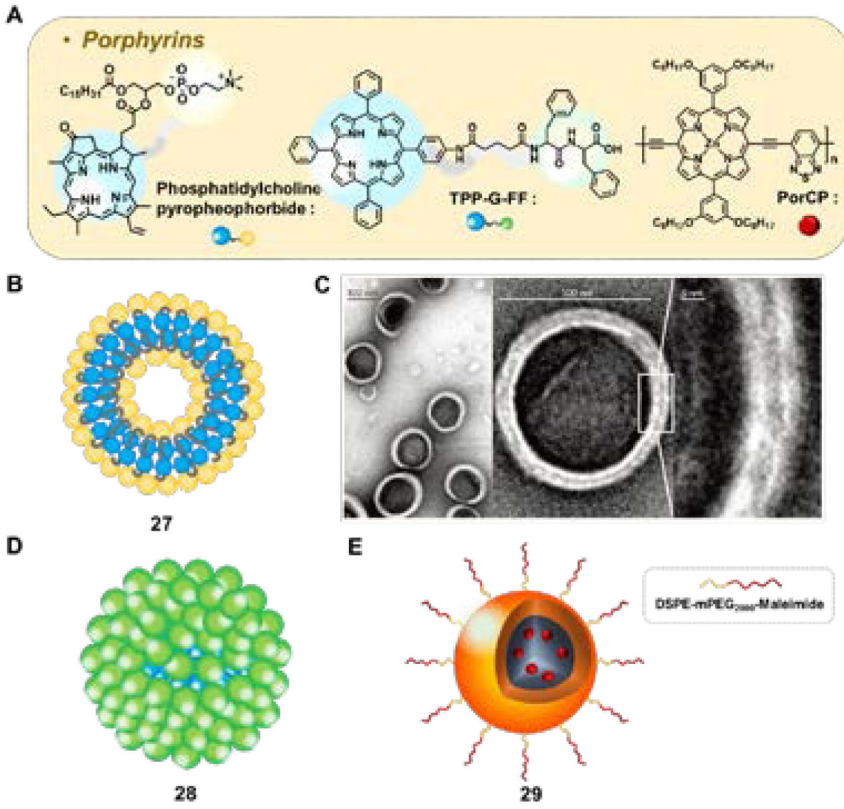

Fig. 7.

(A) Molecular structure of porphyrins: phosphatidylcholine-pyropheophorbide, TPP-G-FF, and PorCp, and (B) phosphatidylcholine-pyropheophorbide's modified porphysome **27**. (C) Transmission electron microscopy images of **27**. Reprinted by permission from Macmillan Publishers Ltd: Nature Materials (Ref. 32), Copyright 2011. (D) TPP-G-FF self-assembled porphyrins **28** and (E) PorCP polymeric nanoprecipitates **29**. TPP-G-FF: tetraphenylporphyrin conjugate; PorCp: porphyrin conjugated polymer.

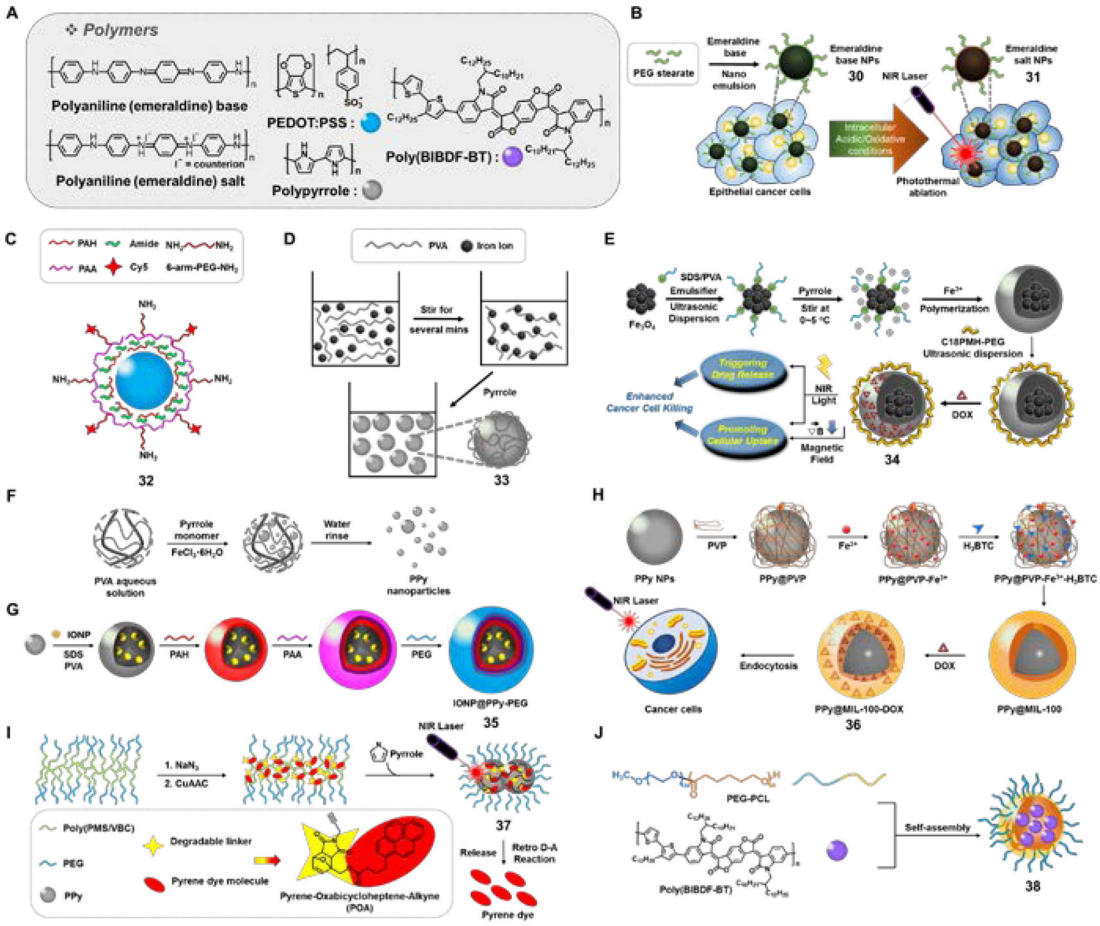

Fig. 8.

(A) Molecular structure of polymers explored in the context of PTT: Polyaniline, PEDOT:PSS, polypyrrole (PPy), and poly(BIBDF-BT). (B) Systematic process for polyaniline (emeraldine) base nanoparticle **30** and polyaniline (emeraldine) salt nanoparticle **31**. (C) Structure of PEDOT:PSS-PEG nanoparticle **32**. (D) Systematic illustration of PVA-coated PPy nanoparticles **33**, (E) Fe_3O_4-PPy-PEG nanoparticles **34**, (F) PPy nanoparticles by a simple one-step aqueous dispersion polymerization method, (G) IONP@PPy-PEG nanoparticles **35**, (H) multifunctional PPy@MIL-100-DOX nanoparticle **36,** (I) PEG-POA PPy nanoparticle **37**, and (J) poly(BIBDF-BT) nanoparticles **38**. PEDOT:PSS: poly(3,4-ethylenedioxythiophen):poly(4-styrene-sulfonate); PVA: poly(vinylalcohol); IONP: iron-oxide nanoparticles.

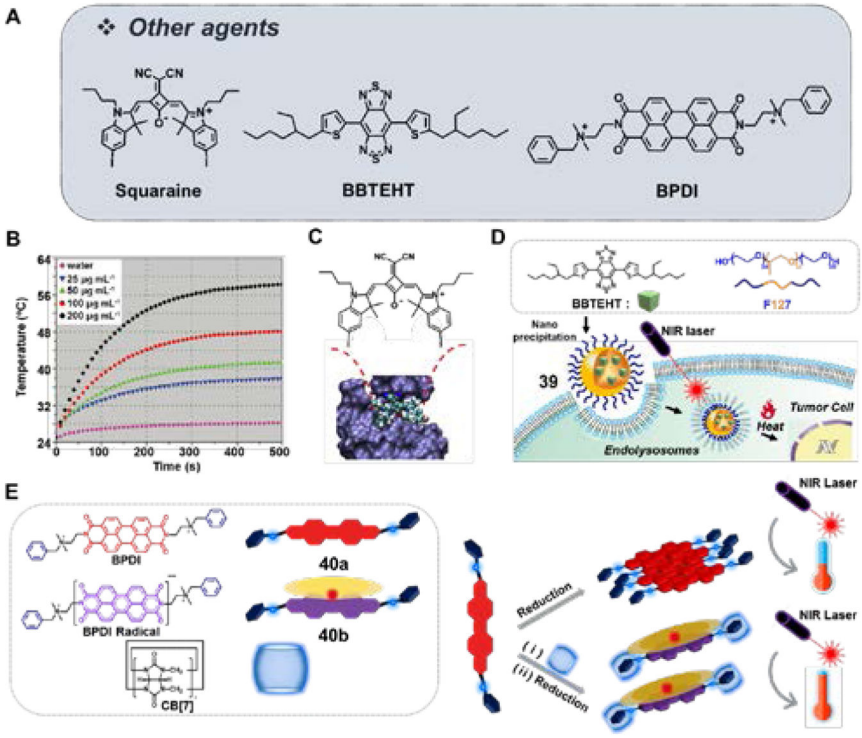

Fig. 9.

(A) Molecular structure of other agents studied in the context of PTT: Squaraine, BBTEHT, and BPDI. (B) Temperature elevation of water and aqueous melanin-dopamine CNSs at different concentrations seen upon NIR light illumination (808 nm laser, power 2 W/cm^2). Reproduced from Ref. 47 with permission from Wiley. (C) Molecular structure of squaraine with BSA adduct. Reproduced from Ref. 48 with permission from Elsevier. (D) Molecular structure of BBTEHT and its self-assembled nanoparticles **39**. (E) Molecular structure of BPDI **40a**, BPDI radical species **40b**, CB[7]-based molecular assembly. Also shown is the chemical reduction and corresponding photothermal conversion seen upon NIR irradiation. BBTEHT: benzo[1,2-c;4,5-c′]bis[1,2,5]thiadiazole-4,7-bis(5-(2-ethylhexyl)thiophene); BPDI: 1:2 bola-type amphiphilicperylene diimide.

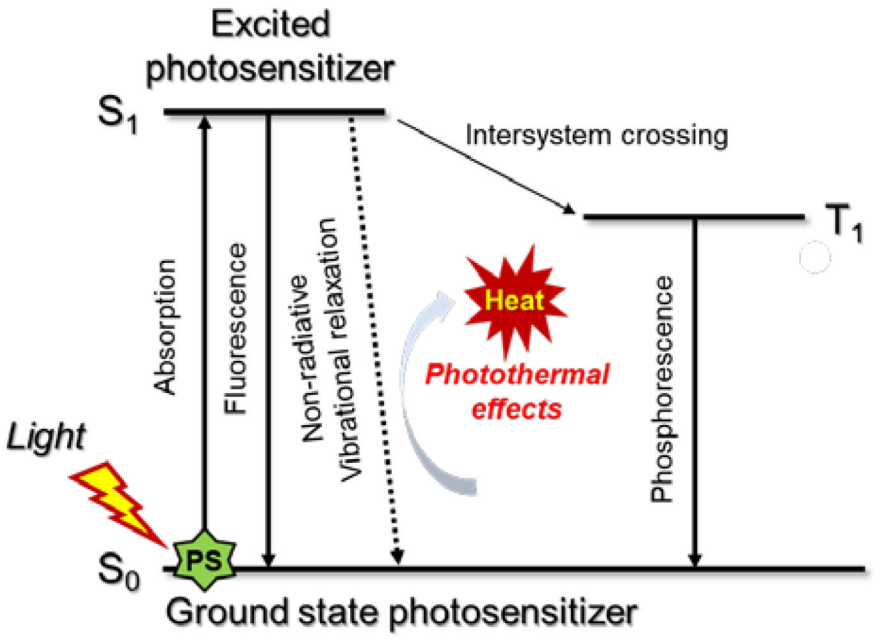

Scheme 1.

Working principle underlying organic PTT agents as illustrated using a modified Jablonski diagram.

Table 1

Organic photothermal agents for cancer therapy

Category	Probe construction	Laser irradiation	Photothermal effect	Therapeutic strategy	Ref.
Indocyanine green	ICG/DMPC liposomes (**1**)	808 nm (1.1 W/cm^2, 1 min)	Increase by ~15 °C from 25 °C (H_2O, n.d.)	Passive targeting (EPR)	8
Indocyanine green	ICG/PL-PEG aggregates (**2**)	808 nm (1.25 W/cm^2, 2 min)	ΔT = ~22 °C (H_2O, 0.05 mg/mL)	Active targeting (FA or mAb)	9
Indocyanine green	ICG/PLGA/cancer cell membrane shell nanoparticles (**5**)	808 nm (1.0 W/cm^2, 8 min)	Increase by ~49.2 °C from 25 °C (PBS, n.d.)	Passive targeting (EPR)/ Homologous active targeting (cancer cell membrane shell)	10
Indocyanine green	ICG/DOX/PLGA/lecithin/PEG nanoparticles (**6**)	808 nm (1.0 W/cm^2, 5 min)	Increase to ~53.2 °C (PBS, n.d.)	Passive targeting (EPR)/ Chemo-photothermal combination therapy	11
Heptamethine cyanine	IR825/PEG micelles (**7**)	808 nm (0.5 W/cm^2, 5 min)	ΔT = ~45 °C (H_2O, 0.5 mg/mL)	Passive targeting (EPR)	12
Heptamethine cyanine	IR780/heparine/FA nanoparticles (**8**)	808 nm (0.6 W/cm^2, 2 min)	Increase by ~19 °C from 23 °C (H_2O, 10 μg/mL)	Active targeting (FA ligand)/Improved bio-applicability in heparine	13
Heptamethine cyanine	4-hydroxybenzoic acid-appended heptamethine (**9**)	808 nm (1.5 W/cm^2, 2 min)	Increase by ~28 °C from 28 °C (H_2O, n.d.)	Mitochondrial targeting	14
Heptamethine cyanine	Amine-functionalized heptamethine (**10**)	750 nm (6.0 W/cm^2, 2 min)	Increase by ~37 °C from 25 °C (pH 7.4 buffer, 10 μM) Increase by < 10 °C from 25 °C (pH 2.4 buffer, 10 μM)	pH-controlled	15
Phthalocyanine	GdSand/HDL/Tat nanoparticles (**11**)	770 nm (1500 mW, 3 min)	Increase by ~7 °C from 37 °C (PBS, OD_{770}=0.24, 0.79)	Tat mediated cell uptake/ Improved bio-applicability in HDL	18
Phthalocyanine	$PcBu_4$/Pluronic F-68/glycol chitosan/heparin nanoparticles (**12**)	671 nm (6.4 W/cm^2, 3 min)	Increase by ~32 °C from 25 °C (H_2O, n.d.)	Passive targeting (EPR)/ Improved bio-applicability	19
Phthalocyanine	SiNcOH/DSPE/PEG(NH_2) nanoparticles (**13**)	808 nm (1.5 W/cm^2, 12 min)	Increase by ~26.7 °C from 26 °C (H_2O, 150 ppm)	Passive targeting (EPR)	20
Phthalocyanine	SiNc2/PPI G5/PEG nanoparticles (**14**)	785 nm (1.3 W/cm^2, 5 min	Increase by ~39 °C from 25 °C (PBS, 100 μg/mL)	Passive targeting (EPR)/ Improved bio-applicability in PPI G5-PEG	21

Category	Probe construction	Laser irradiation	Photothermal effect	Therapeutic strategy	Ref.
Hemicyaninerhodamine	RC/BSA (**15**)	915 nm (1.0 W/ cm^2, 10 min)	Increase by ~26 °C from 23 °C (H_2O, 0.1 mM)	Improved bio-applicability	22
Cryptocyanine	Cryptocyanine/TPP (**16**)	730 nm (3.0 W/ cm^2, 5 min)	ΔT = ~24.5 °C (DMSO, 0.5 mM)	Mitochondrial targeting	23
Diketopyrrolopyrrole	DPP-TPA nanoparticles (**17**)	660 nm (1.0 W/ cm^2, 10 min)	Increase by ~35 °C from 25 °C (PBS, 80 μg/mL)	Passive targeting (EPR)	24
Diketopyrrolopyrrole	SDPP nanoparticles (**18**)	660 nm (1.0 W/ cm^2, 10 min)	Increase by ~35 °C from 25 °C (PBS, 40 μg/mL)	Passive targeting (EPR)	25
Diketopyrrolopyrrole	SP4/DSPE-$mPEG_{2000}$ nanoparticles (**21**)	808 nm (0.24 W/cm^2, 4 min)	Increase by ~23 °C from 22 °C (PBS, 20 μg/mL)	Passive targeting (EPR)	26
Diketopyrrolopyrrole	PDPP/Pluronic F127 nanoparticles (**22**)	808 nm (1.0 W/ cm^2, 10 min)	ΔT = ~20 °C (H_2O, 40 ppm)	Passive targeting (EPR)	27
Croconaine	Croc	780 nm (3.5 W/ cm^2, 10 min)	ΔT = ~10 °C (MeOH: H_2O 4:1, 2 μg/mL)	n.d.	28
Croconaine	Croc	830 nm (3.5 W/ cm^2, 10 min)	ΔT = ~2 °C ($CHCl_3$, 4 μg/mL)	n.d.	28
Croconaine	CrocRot I	830 nm (3.5 W/ cm^2, 20 min)	ΔT = ~10 °C ($CHCl_3$, 4 μg/mL solution of **25** and addition of 50 eq. macrocycle at 10 min)	n.d.	28
Croconaine	CrocRot II	808 nm (3.5 W/ cm^2, 10 min)	ΔT = ~7 °C ($CHCl_3$, n.d.)	n.d.	29
Croconaine	CrocRot II/Pluronic F127/silicate nanoparticles (**23**)	830 nm (3.5 W/ cm^2, 20 min)	ΔT = ~12 °C (H_2O, n.d.)	n.d.	29
Croconaine	Dumbbell Croc/Pluronic F127/silicate nanoparticles (**24**)	808 nm (3.5 W/ cm^2, 20 min)	ΔT = ~7 °C (H_2O, n.d.)	n.d.	30
Croconaine	Dumbbell Croc/PLGA/DSPE-$mPEG_{2000}$ nanoparticles (**25**)	808 nm (n.d., 15 min)	ΔT = ~15 °C (HEPES, n.d.)	n.d.	30
Croconaine	Dumbbell Croc/DPPC/DSPE-$mPEG_{2000}$ liposomes (**26**)	808 nm (6.0 W/ cm^2, 5 min)	ΔT = ~45 °C (HEPES, n.d.)	n.d.	30
Croconaine	CrocRot IV	808 nm (3.5 W/ cm^2, 15 min)	ΔT = ~10 °C (pH 5.0) ΔT = ~4 °C (pH 6.5) ΔT = < 1 °C (pH 7.4)	n.d.	31

Category	Probe construction	Laser irradiation	Photothermal effect	Therapeutic strategy	Ref.
Porphyrin	Phosphatidylcholine-pyropheophorbide/DSPE-mPEG$_{2000}$/cholesterol porphysomes (**27**)	658 nm (1.9 W/cm^2, 1 min)	Increase by ~30 °C from 30 °C (tumor tissue)	Passive targeting (EPR)/ Cholesterol mediated tumor accumulation	32
Porphyrin	Phosphatidylcholine-pyropheophorbide/DSPE-mPEG$_{2000}$/cholesterol porphysomes (**27**)	671 nm (750 mW, 100 J/cm^2)	Increase by ~40 °C from 30 °C (tumor tissue)	Passive targeting (EPR)/ Cholesterol mediated tumor accumulation	33
Porphyrin	TPP-G-FF nanodots (**28**)	635 nm (1.2 W/cm^2, 10 min)	Increase by ~35 °C from 25 °C (H_2O, 0.8 mg/mL)	n.d.	34
Porphyrin	PorCP/DSPE-mPEG$_{2000}$-Maleimide nanoparticles (**29**)	808 nm (0.75 W/cm^2, 10 min)	Increase by ~52 °C from 24 °C (H_2O, 0.1 mg/mL)	Passive targeting (EPR)/ HIV-Tat mediated cell uptake	35
Polyaniline	Polyaniline(emeraldine)/PEG-stearate nanoparticles (**30**)	808 nm (2.45 W/cm^2, 3 min)	Increase by ~40 °C from 28 °C (H_2O, 0.5 mg/mL)	Passive targeting (EPR)	37
Polyaniline	PEDOT:PSS/PEG nanoparticles (**32**)	808 nm (1.0 W/cm^2, 5 min)	Increase by ~35 °C from 16 °C (H_2O, 0.1 mg/mL)	Passive targeting (EPR)	38
Polypyrrole	Polypyrrole/PVA nanoparticles (**33**)	808 nm (0.5 W/cm^2, 5 min)	Increase by ~30 °C from 15 °C (H_2O, 0.1 mg/mL)	Passive targeting (EPR)	39
Polypyrrole	Polypyrrole@Fe_3O_4/PEG/DOX nanoparticles (**34**)	808 nm (0.75 W/cm^2, 5.5 min)	ΔT = ~22 °C (H_2O, 0.5 mg/mL)	Passive targeting (EPR)/ Chemo-photothermal combination therapy	40
Polypyrrole	Polypyrrole/PVA nanoparticles	808 nm (2.0 W/cm^2, 10 min)	Increase by ~34.5 °C from 21 °C (RPMI-1640 culture medium, 30 μg/mL)	Passive targeting (EPR)	41
Polypyrrole	Polypyrrole@Fe_3O_4 nanoparticles	808 nm (0.25 W/cm^2, 5 min)	Increase by ~33.5 °C from 22 °C (H_2O, 160 ppm)	Passive targeting (EPR)	42
Polypyrrole	Polypyrrole@IONP/PEG nanoparticles (**35**)	808 nm (1.0 W/cm^2, 5 min)	ΔT = ~40 °C (H_2O, 0.5 mg/mL)	Passive targeting (EPR)	43
Polypyrrole	Polypyrrole@MIL-100/DOX nanoparticles (**36**)	808 nm (2.0 W/cm^2, 5 min)	ΔT = ~34 °C (H_2O, 0.1 mg/mL)	Passive targeting (EPR)/ Chemo-photothermal combination therapy	44
Polypyrrole	Polypyrrole/PEG/POA nanoparticles (**37**)	808 nm (2.0 W/cm^2, 20 min)	Increase of ~50 °C from 22 °C (H_2O, 48 μg/mL)	Passive targeting (EPR)	45
Poly(BIBDF-BT)	Poly(BIBDF-BT)/PEG/PCL/nanoparticles (**38**)	785 nm (1.5 W/cm^2, 5 min)	ΔT = ~65 °C (H_2O, 20 μg/mL)	Passive targeting (EPR)	46

Category	Probe construction	Laser irradiation	Photothermal effect	Therapeutic strategy	Ref.
Dopamine-Melanin	Dopamine/melanin colloidal nanospheres	808 nm (2.0 W/ cm^2, 500 s)	Increase of ~34 °C from 25 °C (H_2O, 0.2 μg/mL)	Passive targeting (EPR)	47
Squaraine	Squaraine/BSA/FA	680 nm (20 W/ cm^2, 10 min)	ΔT = ~22 °C (PBS, 1 mg/mL)	Active targeting (FA ligand)	48
Benzobisthiadiazole	BBTEHT/Pluronic 127 nanoparticles (**39**)	808 nm (1.77 W/cm^2, 20 min)	Increase of ~23 °C from 21 °C (H_2O, 50 μg/mL)	Passive targeting (EPR)	49
Perylene diimide	BPDI/$(CB[7])_2$ (**40**)	808 nm (1.0 W/ cm^2, 10 min)	Increase of ~19.5 °C from 25 °C (H_2O, n.d.)	n.d.	50

[**Abbreviation**] n.d.: not described, ICG: indocyanine green, DMPC: 1,2-dimyristoyl-*sn*-glycero-3-phosphocholine, EPR: enhanced permeability and retention, PL: phospholipid, PEG: polyethylene glycol, FR: folate receptor, mAb: monoclonal antibody, PLGA: poly(lactic-co-glycolic acid), PBS: phosphate buffered saline, DOX: doxorubicin, GdSand: gadolinium-bisnapthalocyanine sandwich complex, HDL: high-density lipoprotein, Tat: transactivator of transcription, $PcBu_4$: tetra-*t*-butylphthalocyanine, SiNcOH: silicon 2,3-naphthalocyanine dihydroxide, DSPE: 1,2-distearoyl-*sn*-glycero-3-phosphoethanolamine, SiNc2: silicon 2,3-naphthalocyanine bis(trihexylsilyloxide), PPI G5: polypropylenimine dendrimer, RC: hemicyanine-rhodamine, BSA: bovine serum albumin, DPP-TPA: dithienyldiketopyrrolopyrrole-triphenylamine, SDPP: 5-bis(6-bromo-hexyl)-3,6-bis[5-[4-(4-dimethylaminobenzoyl)-phenyl]-thiophen-2-yl]-2,5-dihydropyrrolo[3,4-c]pyrrole-1,4-dione, SP: semiconducting polymer, PDPP: poly(dithienyldiketopyrrolopyrrole), DSPE-$mPEG_{2000}$: 1,2-distearoyl-*sn*-glycero-3-phosphoethanolamine-*N*-[methoxy(polyethylene glycol)-2000], Croc: croconaine dye, CrocRot: pseudorotaxane croconaine, HEPES: (4-(2-hydroxyethyl)-1-piperazineethanesulfonic acid), DPPC: 1,2-dipalmitoyl-*sn*-glycero-3-phosphocholine, TPP-G-FF: tetraphenylporphyrin conjugate, PorCp: porphyrin conjugated polymer, HIV: human immunodeficiency virus, PEDOT: poly(ethylenedioxythiophene), PSS: poly(4-styrene-sulfonate), PVA: poly(vinylalcohol), PPy: polypyrrole, MIL: iron(III)carboxylate metal organic framework, POA: pyrene-oxabicycloheptene-alkyne, PCL: poly(ethylene glycol)$_{114}$-*b*-poly(caprolactone)$_{60}$, BIBDF: (3E,7E)-3,7-bis(2-oxoindolin-3-ylidene)benzo-[1,2-b:4,5-b′]-difuran-2,6(3H,7H)-dione, BT: bithiophene, BBTEHT: benzo[1,2-c;4,5-c′]bis[1,2,5]thiadiazole-4,7-bis(5-(2-ethylhexyl)thiophene), BPDI: 1:2 bola-type amphiphilic perylene diimide, CB[7]: Cucurbit[7]uril.